Journal of Applied Volcanology

RESEARCH

Open Access

Tephra fall hazard and exposure analysis at Corbetti volcanic system, Ethiopia: implications for risk management

Julia M Crummy[1*], Yewubinesh Bekele[2,3], Samantha Engwell[1*], Karen Fontijn[4], Elias Lewi[5], Susan C Loughlin[1*], Amdemichael Z Tadasse[6,7,8], Charlotte Vye-Brown[1] and Gezahegn Yirgu[8]

Abstract

The Corbetti volcanic system, located in the central part of the Main Ethiopian Rift, has no recorded eruptions in living memory but shows evidence of past activity ranging from highly explosive Plinian eruptions to dominantly effusive events. Approximately 1.1 million people live within 30 km of the volcano and over 12 million within 100 km, alongside critical infrastructure such as highways, Hawassa Airport, and major towns including Hawassa and Shashemene. A geothermal power plant is also under development within the caldera. Despite significant advances in understanding Corbetti through recent fieldwork, hazard assessment remains limited due to challenges in distinguishing deposits, poor lateral continuity, and scarce dateable material. This study combines new and existing field data with expert judgment to develop probabilistic tephra-fall footprints for four plausible eruption scenarios and a worst-case scenario. These are integrated with exposure data to assess potential impacts and eruption frequency. Results indicate an average recurrence interval of 520 years for any explosive eruption, with low-to-moderate volume events ten times more likely than large Plinian eruptions. Modelling shows tephra dispersal predominantly westward, potentially exposing over 750,000 people, ~3,400 km of roads, and ~1,600 km^2 of cropland to tephra loads exceeding 1 kg m^{-2} (~1.6 mm) during a Plinian-type event. In the same scenario, more than 37,000 people could experience > 100 kg m^{-2} (~16 cm) of tephra within 20 km of the vent. Even smaller eruptions could significantly impact agriculture and infrastructure, underscoring the need for preparedness and risk management in a region with no historical memory of explosive volcanism.

Keywords Corbetti, Tephra hazard, Volcanic exposure, Ashfall impacts, Volcanic hazard

*Correspondence:
Julia M Crummy
juli@bgs.ac.uk
Samantha Engwell
sameng@bgs.ac.uk
Susan C Loughlin
sclou@bgs.ac.uk
[1]British Geological Survey, Lyell Centre, Edinburgh EH14 4AP, UK
[2]Geological Institute of Ethiopia, Addis Ababa, Ethiopia
[3]Institute of Geosciences, University of São Paulo (USP), São Paulo, Brazil
[4]Department of Geosciences, Environment and Society, Université libre de Bruxelles, Brussels, Belgium
[5]Institute of Geophysics, Space Science and Astronomy (IGSSA), Addis Ababa University, Addis Ababa, Ethiopia
[6]Department of Earth Sciences, University of Oxford, Oxford, UK
[7]Lamont-Doherty Earth Observatory, Columbia University, Palisades, New York, USA
[8]School of Earth Sciences, Addis Ababa University, Addis Ababa, Ethiopia

© United Kingdom Research and Innovation as represented by the British Geological Survey 2026. **Open Access** This article is licensed under a Creative Commons Attribution 4.0 International License, which permits use, sharing, adaptation, distribution and reproduction in any medium or format, as long as you give appropriate credit to the original author(s) and the source, provide a link to the Creative Commons licence, and indicate if changes were made. The images or other third party material in this article are included in the article's Creative Commons licence, unless indicated otherwise in a credit line to the material. If material is not included in the article's Creative Commons licence and your intended use is not permitted by statutory regulation or exceeds the permitted use, you will need to obtain permission directly from the copyright holder. To view a copy of this licence, visit http://creativecommons.org/licenses/by/4.0/.

Introduction

Ethiopia is home to nearly half of Africa's Holocene volcanoes, hosting 52 of the continent's 119 identified centres, including five located along its borders with Djibouti and Eritrea (Global Volcanism program 2024; Fig. 1). The majority of Ethiopia's volcanoes are in the Main Ethiopian Rift (MER), the northernmost segment of the East African Rift System, and the Afar Depression. These regions together host a combined population of approximately 21.5 million inhabitants (Ethiopian Statistical Service 2023). Volcanic activity within the MER is diverse, ranging from periods of unrest to dominantly effusive eruptions producing lava flows, to highly explosive eruptions producing extensive tephra fall and pyroclastic density currents (e.g., Yirgu et al. 2014; Vye-Brown et al. 2016; Fontijn et al. 2018). Recent activity in the MER in 2024–2025 at Fentale-Dofen volcanoes was characterised by ground shaking, the opening of fractures, and gas emissions driven by a sequence of dyke intrusions extending up to 50 km and accompanied by hundreds of earthquakes (Way et al. 2025; Lewi et al. 2025). Further north in the Afar Depression, volcanic eruptions have been observed in recent years, including the 23rd November 2025 explosive eruption of the long dormant Hayli Gubbi volcano, whose impact was limited, partly due to low exposure in this remote region, while the dispersed ash caused significant disruptions to global aviation (Limberger et al. 2026). These recent events are good indications that future eruptions from poorly known Ethiopian volcanoes could well cause more disruptions.

Corbetti is an active volcanic system located in the central part of the MER and is the southernmost of the MER central silicic volcanoes. Recent studies have shown that there is evidence of magma accumulation in the crust beneath the Corbetti volcanic system (Biggs et al. 2011; Dambly et al. 2024); however, at the time of writing, there is no active volcano monitoring on Corbetti. Approximately 1.1 million people live within 30 km, and over 12 million people live within 100 km of the Corbetti volcanic system (Jenkins et al. 2024a). Two of Ethiopia's major cities, Hawassa and Shashemene, located within 20 km of Corbetti, are popular tourist destinations, and have populations of over 400,000 and 200,000 people, respectively (Ethiopian Statistical Service 2023). A major

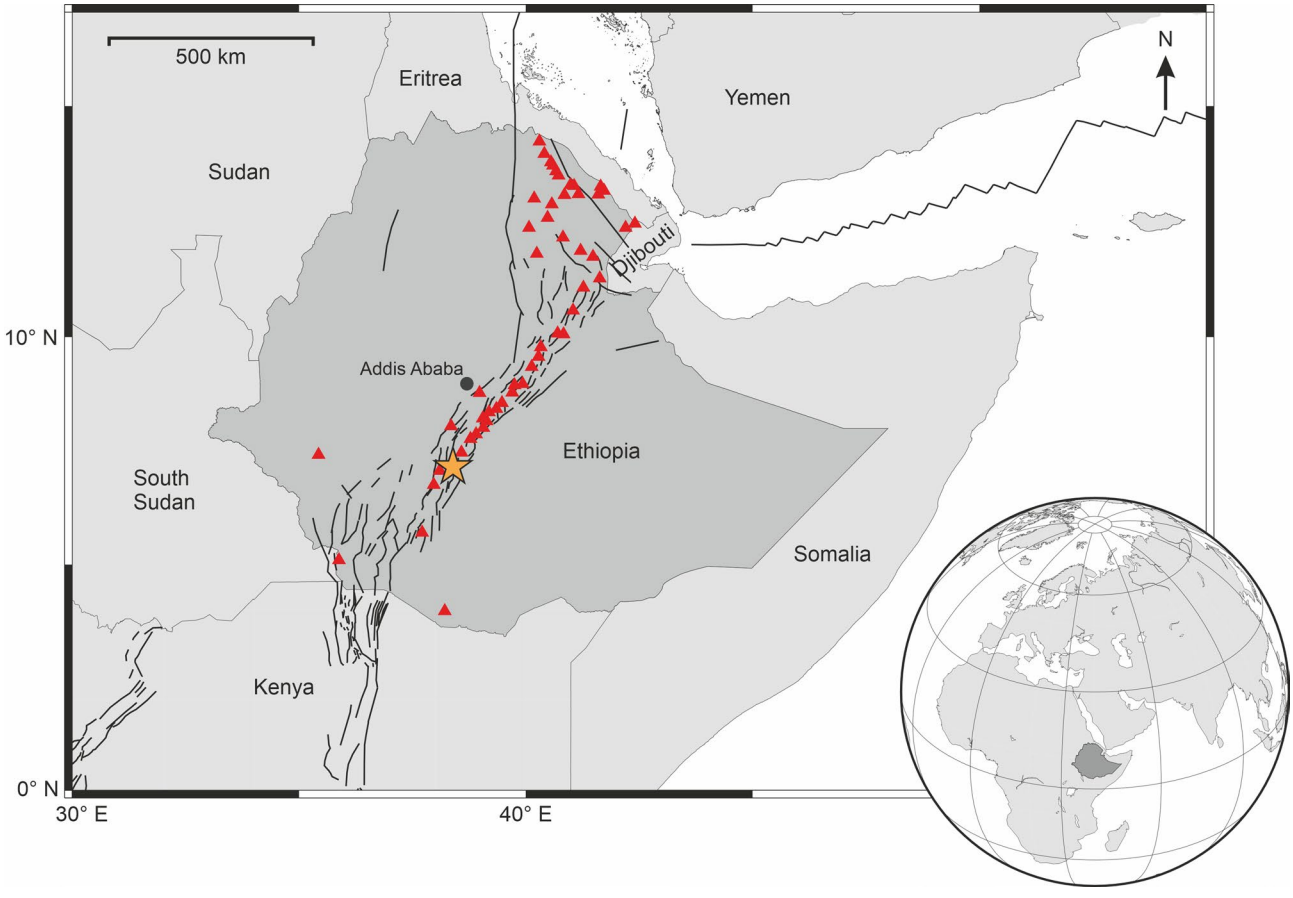


Fig. 1 Map of Ethiopian Holocene volcanoes (triangles) as defined by the Smithsonian institution Global volcanism Program volcanoes of the world database 5.1.0 (Global Volcanism Program 2024, available under the CC-BY-SA 4.0 licence). Thick black lines indicate the location of faults according to the GEM active faults database (Styron and Pagani 2020, available under the CC-BY-SA 4.0 licence). Corbetti volcanic system is highlighted by the star

east-west road crossing Ethiopia passes within 20 km of the volcanic system, and the north-south Trans-African Highway passes through Hawassa and Shashemene (Fig. 2). Hawassa (Awasa) Airport, which has regular daily flights to and from Addis Ababa, is situated just 5 km from the caldera rim and 10 km south-southwest of the central vent. Corbetti caldera is also the location for a new geothermal power plant, which is due to be operational in 2027 (InfraCo Africa 2023). This is a key infrastructure for Ethiopia's move towards greener energy (Benti et al. 2023). Surrounding Corbetti are numerous towns and villages, agricultural land, and road networks. An estimated population of 14,000 people live within the Caldera (Ethiopian Public Health Institute 2021). There is a strong economic dependence on agriculture in this region. As such it is important to understand potential impacts from possible future volcanic activity that may have economic implications for the region.

Recent field campaigns have contributed to a step-change in knowledge from 2015 when the Global Assessment of Risk report (GAR15) highlighted the lack of data on volcanoes in Ethiopia (Brown et al. 2015). Geological and geophysical data acquired in the last decade in the MER (e.g. Yirgu et al. 2014; Hutchison et al. 2016a, 2016b; Rapprich et al. 2016; Vye-Brown et al. 2016; Martin-Jones et al. 2017; Fontijn et al. 2018; McNamara et al. 2018; Siegburg et al. 2018; Clarke et al. 2019, 2020; Tierz et al. 2020; Watts et al. 2020; Colby et al. 2022; Tadesse et al. 2022; Colby 2023; Tadesse et al. 2023a, 2023b; Bedassa et al. 2024; Hilemichaeil et al. 2024; Wuletawu et al. 2024) have increased our understanding of past volcanism and magmatism, particularly at Gedemsa, Bora-Baricha Tullu Moye, Aluto and Corbetti central volcanoes. Since 2014, knowledge of past volcanic activity at Corbetti has significantly increased through extensive field work and data collection (Rapprich et al. 2016; Martin-Jones et al. 2017; Fontijn et al. 2018; Colby et al. 2022). However, for detailed hazard assessments, the data and knowledge are still limited, constrained by difficulties distinguishing between deposits both in the field and geochemically (Fontijn et al. 2018), and lack of lateral continuity of deposits, dateable material and resources to map and correlate volcanic deposits at this complex volcanic system. This study attempts to address some of these knowledge gaps, building on research carried out over the last decade to improve understanding of volcanic activity in the Corbetti volcanic system. Using scenario-based probabilistic tephra fall hazard analysis combined with expert elicitation and exposure data, we highlight and discuss possible impacts from potential future explosive activity. This builds on research to develop methodologies for volcanic hazard assessments in low-data environments

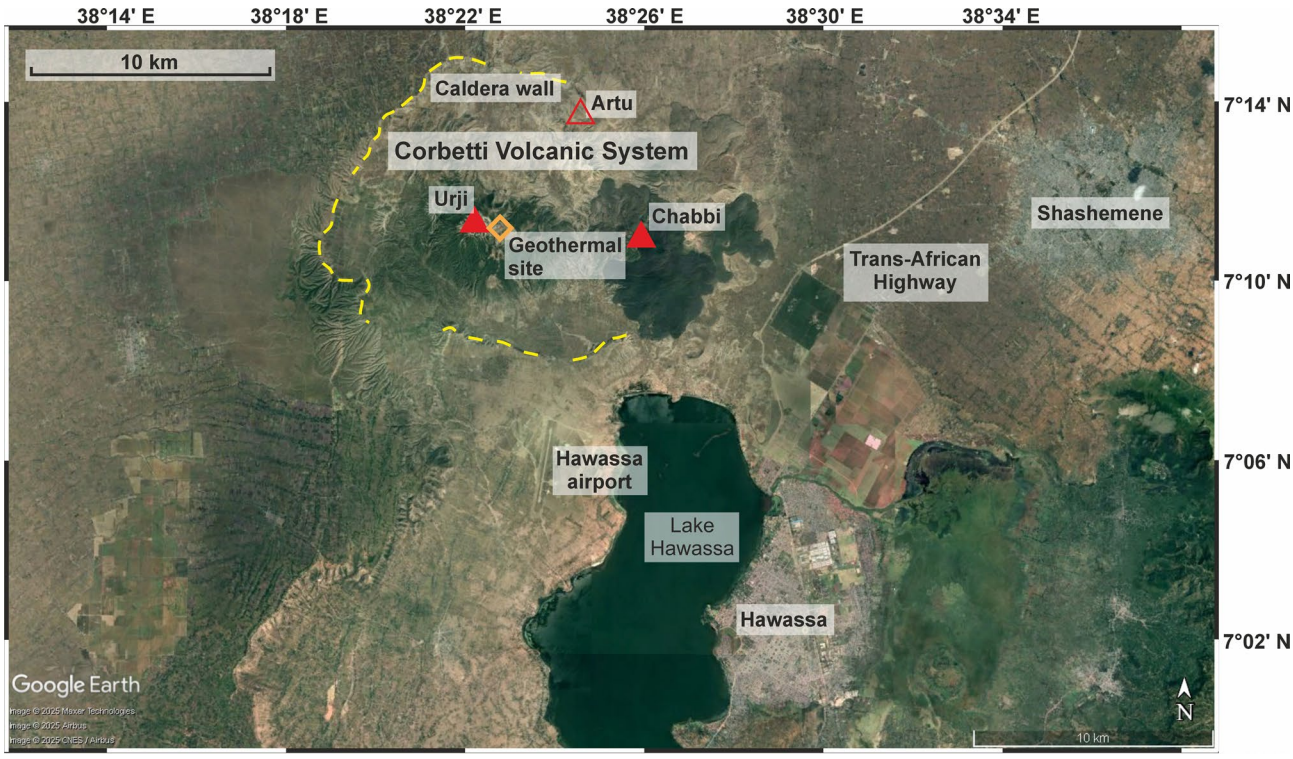


Fig. 2 Map of the Corbetti volcanic system and surrounding area showing the Urji, Chabbi and Artu volcanic centres, the caldera wall (dashed line), and the major towns of Shashemene and Hawassa as well as key infrastructures including the site of the planned geothermal power plant, Hawassa airport and the trans-African highway. Basemap: Google Earth © 2025 Maxar Technologies/Airbus/CNES/Airbus

(Vye-Brown et al. 2019; Jenkins et al. 2024a), and research carried out in the NERC-funded RiftVolc project (2014–2021).

We build on insights on past eruptive activity from previous studies, complimenting these with new field data to derive scenarios of possible future explosive events. We use probabilistic tephra fall modelling to produce maps of tephra accumulation on the ground for each scenario, which we integrate with global exposure data and expert elicitation to discuss the possible tephra fall impacts resulting from potential future events at Corbetti volcanic system.

We hope that this first detailed tephra fall hazard analysis for the Corbetti volcanic system will raise awareness of possible impacts from explosive volcanic activity, and support planning and preparedness for potential future explosive activity in Ethiopia.

Corbetti volcanic system eruptive history

The Corbetti volcanic system developed through a series of caldera-forming eruptions, the last of which occurred approximately 180 ka forming the current Corbetti caldera (Di Paola 1971; Rapprich et al. 2016; Hutchison et al. 2016b; Colby et al. 2022). Post-caldera activity is characterised by explosive pyroclastic activity and the formation of obsidian lava flows (Colby et al. 2022). Within the caldera there are three main volcanic centres: Artu, Urji (Wendo Koshe) and Chabbi (also known as Chabi or Chebi; Fig. 2). Based on morphology and field relationships, Artu is assumed to be the oldest with more recent activity alternating between predominantly effusive activity at Chabbi and explosive activity at Urji (Rapprich et al. 2016; Fontijn et al. 2018). Multiple vents have been identified on the flanks of Urji and Chabbi, suggesting that the edifices formed through multiple polygenetic eruptions (Colby et al. 2022). However, the chronology of the eruptions forming these events and their relationships to each other are unknown (Colby et al. 2022).

Within the Corbetti caldera there are at least two widespread pumice fall deposits (Fig. 3a): the Wendo Koshe Younger Pumice (WKYP) and the Bedded Pumice, separated by small-scale pyroclastic density current and fall deposits (Fontijn et al. 2018; Colby et al. 2022). The Wendo Koshe Older Pumice (WKOP; Fig. 3b) is found at a small number of locations outside the caldera (Rapprich et al. 2016). The Bedded Pumice deposit can be identified at multiple locations within the caldera and is characterised by the presence of obsidian clasts. The relationship of the WKOP to the Bedded Pumice is unknown. The most widespread pumice fall deposit is the WKYP that can be traced towards the east (Fig. 3c), across an area of over 1,040 km^2 (Rapprich et al. 2016). Fontijn et al. (2018) estimated a minimum total erupted bulk volume of 1.3 km^3 for the WKYP deposit using the Pyle (1989) method, with an estimated thickness of 0.5 m in the town of Shashemene, approximately 20 km to the east of Corbetti. The age of the WKYP eruption has been constrained at <2.3 ka cal BP (396 ± 38 BC) based on radiocarbon dating of an underlying palaeosol (Rapprich et al. 2016). Two smaller-scale explosive eruptions followed the WKYP eruption, and at least four obsidian flows from Chabbi have been identified that are stratigraphically younger than the WKYP deposit (Colby et al. 2022).

Martin-Jones et al. (2017) analysed sediment cores from Lake Tilo, 40 km west of Corbetti caldera. Based on geochemical analysis, they identified 12 tephra layers within the last 10,000 years sourced from Corbetti volcanic system. The youngest tephra layer attributed to Corbetti was dated at 1.3–0.5 ka suggesting at least one post WKYP explosive eruption.

Off the flanks of the Corbetti caldera, there are monogenetic cones, which have produced scoria, pyroclastic density currents and lava flows. Colby et al. (2022)

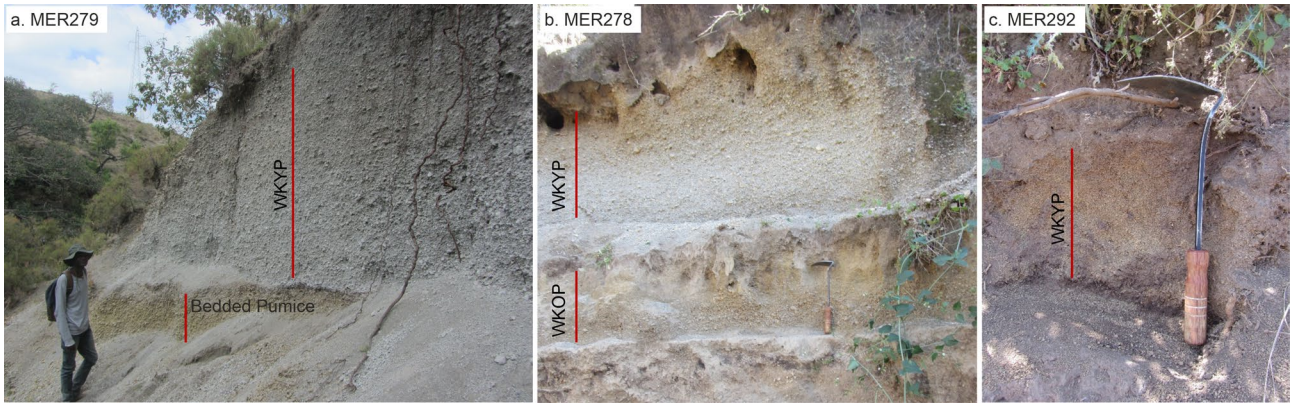


Fig. 3 a. The Wendo Koshe younger pumice (WKYP) overlying the Bedded pumice within the Corbetti caldera, 2.5 km north of the source vent; b. The WKYP overlying the Wendo Koshe older pumice (WKOP) 10 km north of the source vent, and c: distal WKYP 32 km east of the source vent. See fig. 5 for deposit locations (a. MER279; b. MER278; c. MER292)

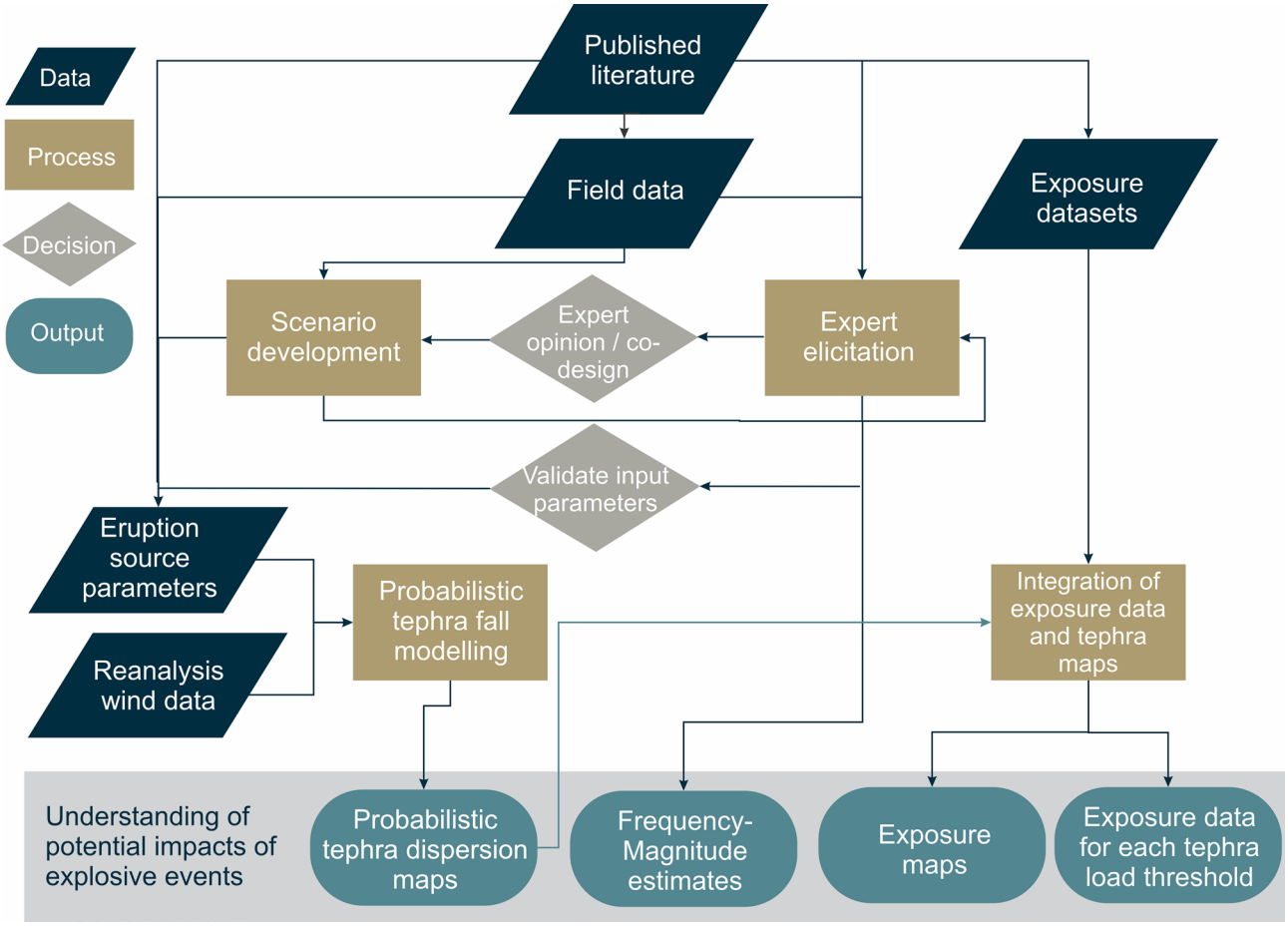


Fig. 4 Flow diagram demonstrating the methodology combining published, field, numerical modelling and expert elicitation data to carry out a tephra fall hazard and exposure analysis

identified and dated (<7375 ± 54 cal BP) a vent close to Lake Hawassa that produced a highly explosive phreatomagmatic eruption resulting in tephra fallout (over 5 km distance) and extensive pyroclastic density currents.

Building on previous studies (Rapprich et al. 2016; Fontijn et al. 2018; Martin-Jones et al. 2017), Colby et al. (2022) identified five to six explosive and effusive eruptions in the last ~2,300 years (since WKYP) estimating a recurrence rate of one eruption every 300–400 years. Based on terrestrial and lacustrine tephra deposits, Martin-Jones et al. (2017) and Fontijn et al. (2018) previously estimated recurrence rates of 900 years and 700–1000 years, respectively, for explosive eruptions.

In 2015, a tephra fall hazard assessment was carried out for selected volcanoes in sub-Saharan Africa, including Corbetti (Jenkins et al. 2024a). Given a lack of data at Corbetti at that time, the nearby, better studied Aluto volcano in the MER was used as an analogue. An expert elicitation yielded an average recurrence interval of 308 years for any Volcanic Explosivity Index (VEI), and 950 and 3600 years for a VEI 3 and VEI 4 explosive event, respectively. Our study builds on Jenkins et al. (2024a), incorporating research carried out on Corbetti in recent years to better understand tephra hazard at Corbetti volcanic system.

Methodology

To work towards understanding volcanic risk at Corbetti volcanic system, we combined published literature and field data to derive potential future explosive event scenarios (Fig. 3). The scenarios were refined through consultation with experts during an elicitation workshop, and used to carry out probabilistic tephra dispersion modelling. The resultant tephra fall footprints were integrated with exposure data to get an understanding of possible impacts from potential future explosive activity at Corbetti volcanic system. We drew on expert knowledge to determine frequency and magnitude estimates for potential explosive events, and to understand uncertainty surrounding these.

The focus of this hazard analysis is on the tephra fall footprint, exposure, and potential impacts. We acknowledge that this only considers a single hazard, and any future explosive activity would likely produce multiple

interrelated hazards including gas emissions and pyroclastic density currents. We also acknowledge that vulnerability, a key component of risk, has not been included in this study.

Explosive event scenarios

There is field evidence of numerous low-to-moderate magnitude pumice cone-forming eruptions within Corbetti caldera, as well as larger magnitude explosive eruptions, including the WKYP deposit described above. There is also evidence of off-edifice explosive phreatomagmatic eruptions, which, due to the high population densities and development along the edges of Lake Hawassa, could have a significant impact on the local and tourist populations. Based on this, four explosive eruptive event scenarios were designed for Corbetti volcanic system representing reasonable likely scenarios and a worst-case scenario, enabling us to explore potential impacts from tephra fall:

- Scenario 1: a low-to-moderate volume event (VEI 3) such as an explosive Vulcanian type event;
- Scenario 2: a large volume event (VEI 4) such as a sub-Plinian to Plinian type eruption;
- Scenario 3: a large volume caldera forming eruption (VEI 6);
- Scenario 4: a phreatomagmatic, off-edifice event (VEI 2 or 3) in the vicinity of Lake Hawassa.

Large magnitude caldera forming eruptions have occurred in the past (Di Paola 1971; Rapprich et al. 2016); therefore, although the likelihood of such an eruption in the future may be small, we believe it should be considered as a reasonable worst-case scenario.

Expert elicitation

A key part of the tephra fall hazard analysis for Corbetti volcanic system requires a judgement of the likely characteristics and recurrence intervals of future explosive eruptions. Estimating eruption magnitudes (volume of magma erupted) is subject to significant uncertainties due to factors such as limited exposure of deposits, uncertainties in deposit thickness and difficulties correlating deposits (e.g. Constantinescu et al. 2022). Eruption frequencies are also subject to uncertainties for the same reasons and because across the Corbetti volcanic system there is limited material available and suitable for dating (Fontijn et al. 2018). Such information is nevertheless crucial to understand and model future volcanic hazards, both in time and space.

To support the information derived from field data, we elicited the judgement of a group of five experts, using the SHeffield ELicitation Framework (SHELF; Oakley and O'Hagan 2010), on the recurrence rate of future explosive silicic eruptions at Corbetti volcanic system (Crummy et al. 2018). Experts were invited based on their knowledge and experience of working in the Main Ethiopian Rift. Readers are referred to Crummy et al. (2018) for details.

The SHELF method is a rapid elicitation approach typically carried out in a half-day workshop, limiting the number of experts and questions to focus discussion between the experts – a key part of the process (Williams et al. 2021). Unlike other elicitation methods used in volcanology, such as the Cooke method (Aspinall et al. 2006), experts are not weighted based on their knowledge and experience or performance on seed questions (Aspinall 2021; Bernard et al. 2024). SHELF aims, after an elicitation of individual opinions, to form a group aggregate view through discussion (O'Hagan 2019). The final probability distribution represents the group consensus and one that a rational independent observer might form having witnessed the discussions and accounted for the views of all the experts.

To derive information on the frequency of potential future eruptions at Corbetti volcanic system, the following questions were elicited:

1. In a 100,000-year period, how many silicic eruptions of any size would you expect at the volcano in question?
2. For the same volcano, given 10,000 realisations of a future silicic volcanic eruption, how many would be an 'explosive Vulcanian' type eruption (e.g., VEI 3, total erupted tephra volume 0.01 to 0.1 km^3)?
3. For the same volcano, given 10,000 realisations of a future silicic volcanic eruption, how many would be a 'sub-Plinian' to 'Plinian' type eruption (e.g., VEI 4, total erupted tephra volume 0.1 to 1 km^3)?

The recurrence rate of any silicic eruption for the Corbetti volcanic system was calculated from the elicited response on the number of silicic eruptions of any type in a 100,000-year period (Crummy et al. 2018). The frequency of each eruption type was determined by randomly simulating 10,000 realisations from each elicited distribution. The proportion of each type of eruption was assumed to be independent of the total number of eruptions. It should be noted here that there is a suite of explosive event types not included in the 'explosive Vulcanian' (VEI 3) and 'sub-Plinian' to 'Plinian' (VEI 4) eruption types elicited.

In addition to the elicitation, consultation was carried out with the experts on the explosive event scenarios and feedback was sought on our eruption source parameters for probabilistic inversion modelling and tephra fall hazard analysis. These included the explosive event scenarios, vent location, eruption column height and total erupted volume ranges for each scenario, particle size

distribution and particle density. This enabled us to refine the modelling input parameters validated through the experts.

Tephra fall hazard analysis

To carry out a tephra fall hazard analysis, we used new and existing field and numerical modelling data to estimate eruption source parameters for explosive events using a scenario-based approach for probabilistic numerical modelling.

Field data

Tephra thickness information for the WKYP has been previously published by Fontijn et al. (2018). We supplement this thickness data with grain size information collected for the same deposit during a joint field campaign (November 2017; Supplementary data). Deposits across the dispersal axis were sampled (whole deposit) and sieved by hand in 1 phi increments (each phi representing a doubling or halving of the particle size). Clasts greater than −1 phi (2 mm) were separated according to their componentry.

Inversion modelling of WKYP pumice

Probabilistic inversion modelling on the WKYP deposit was carried out using the *Tephra2* dispersion model (Bonadonna et al. 2005a). *Tephra2* is widely used to invert field data to estimate the total erupted volume, the eruption column height and the tephra fall footprint of the eruption (e.g., Hasenaka et al. 2011; Fontijn et al. 2011; Fernandez-Turiel et al. 2015; Yang et al. 2021; Brown et al. 2022; Scollo et al. 2025). *Tephra2* calculates the total mass per unit area (kg m^{-2}) of tephra accumulation at individual grid locations by solving a simplified mass conservation equation based on the work of Suzuki (1983). The mass conservation equation considers the distribution of tephra mass in the eruption column and particle settling velocity, as well as horizontal diffusion within the eruption column and atmosphere after the particle has been ejected from the plume (Connor et al. 2001; Bonadonna et al. 2005a; Connor and Connor 2006). We ran 1000 simulations for the WKYP deposit to obtain the best-fit eruption source parameters that minimise errors between the measured tephra characteristics and model outputs.

Probabilistic tephra fall hazard analysis

Tephra dispersion modelling was carried out for the four explosive event scenarios using *TephraProb*, a freely available Matlab package developed to produce probabilistic hazard assessments for tephra fallout (Biass et al. 2016). *TephraProb* uses the *Tephra2* code to produce probabilistic maps of tephra accumulation on the ground for a given set of input parameters. We ran 1000 simulations per scenario, which stochastically sampled the eruption source and modelling parameters to produce individual modelled scenarios. *TephraProb* then processes them to produce probability of exceedance outputs (probability maps, hazard curves and probabilistic isomass maps) given thresholds of tephra accumulations per scenario. The exceedance probability for a given threshold is determined by calculating the proportion of simulations that exceeds this value at each pixel. The reader is referred to Biass et al. (2016) for a comprehensive description of *TephraProb*.

Tephra load thresholds of 1, 10 and 100 kg m^{-2} (250 and 500 kg m^{-2} were included for a VEI 6 event), approximately equivalent to 1-, 10- and 100-mm thickness were used to quantify exposure to people and roads, infrastructure, and the onset of damage to weak buildings (Blong 2003; Jenkins et al. 2014, 2015; Blake et al. 2017; Hayes et al. 2022; Table 1).

Modelling input parameters

Input parameters required by *Tephra2* and *TephraProb* include eruption source parameters, model parameters, and wind data. These are provided in Table 2 and described in detail below. All input parameters were validated and refined through discussion during the expert elicitation workshop.

Vent Location: Previous studies have identified multiple vents on the flanks of Urji and Chabbi (Colby et al. 2022). These have not been mapped in detail, correlated with pyroclastic deposits or dated (Colby et al. 2022), therefore a vent susceptibility map is not possible with the current state of knowledge. To reflect the distribution of vents, we have selected vent locations at both volcanic centres. Chabbi has typically produced lower volume explosive activity than Urji, therefore for scenario 1, a low-moderate volume silicic event, we chose a vent location on the flanks of Chabbi, close to high population densities. For the larger volume explosive events of scenarios 2 and 3 we selected a central vent location on Urji within the caldera (the assumed vent of the WKYP eruption; Rapprich et al. 2016). For scenario 4 we have selected a vent location close to Lake Hawassa (Biftu Tuff cone after Colby et al. 2022) to demonstrate potential impacts from a vent close to more densely populated areas.

Grain Size Distribution: Due to deposit exposure, WKYP samples were collected at either very proximal (<5 km) or distal (15–30 km) locations (Fig. 5); therefore, a total grain size distribution could not be determined. However, input grain size distribution was informed by field measurements (supplementary data): for scenarios 1, 2 and 3 we assume a normal grain size distribution (GSD) with maximum and minimum bounds of −6 phi (64 mm) and 7 phi (8 µm), respectively, with a median between −1 and 2 phi and standard deviation of 1 to 2

Table 1 Tephra fall impacts adapted from Jenkins et al. (2015)

	1–10 mm	10–100 mm	100–1,000 mm
Public health	Irritation of eyes/airways; Exacerbation of pre-existing conditions Stress related to increased workload and uncertainty about long-term effects	Similar effects as for 1–10 mm, but greater proportion of population affected; Ash remobilisation may prolong effects	Casualties from tree/building collapse; Prolonged exposure: increased stress, increased risk of chronic silicosis and inflammatory responses; Prolonged or permanent relocation possible
Infrastructure	Traction/visibility problems; Possible airstrip closure; Engine/brake wear; Clogging of air-and-water handling and filtration systems; Blockages of water intake structures; Abrasion damage to electrical and mechanical equipment	Traction/visibility problems; Airstrip closed; Power line and weak structure collapse; Blockages drains/ditches/sewers	Severe transport effects; Remobilisation/drifting; Loading on bridges; Disruption to generation plants; High risk of severe damage to water and waste treatment plants
Buildings	No structural damage; Possible abrasion of roofs; Possible corrosion of metallic components	Damage to non-structural elements; Infiltration ash into interiors; Potential collapse of non-engineered and long-span roofs	Non-engineered, long span and low-pitched roofs vulnerable to collapse
Clean-up	Minor clean-up required (roofs/gutters, sweeping roads); High water demand for clean-up	Co-ordinated clean-up of roads, paved areas; Private properties requiring assistance with clean-up and disposal; Ash-dumps needed	Greater resources and time for repeated and frequent clean-up needed; Vegetated areas may require cleaning
Economy	Disruption to work/travel; Clean-up cost; Increased maintenance costs; Possible increase in volcano-tourism	Repeated ash falls/remobilisation impact health and hence business	Losses associated with business disruption, reconstruction, relocation; Loss of land

Table 2 Eruption source and modelling input parameters for the *Tephra2* inversion (WKYP inversion) and *TephraProb* (scenarios 1–4) probabilistic modelling. Note that *TephraProb* uses the *Tephra2* code; therefore, the required modelling input parameters are the same. However, some of the inputs for the *Tephra2* inversion require ranges, whereas *TephraProb* requires a single value input

Input parameter	WKYP Inversion	Scenario 1 (VEI 3)	Scenario 2 (VEI 4)	Scenario 3 (VEI 6)	Scenario 4 (VEI 2/3)
Vent					
Vent easting	430222	437986	430316	430316	439500
Vent northing	795022	791516	795089	795089	789800
Vent UTM zone	37	37	37	37	37
Vent height *(m a.s.l.)*	2320	2000	2320	2320	1700
Eruption					
Minimum total erupted mass *(kg)*	1×10^{10}	6.2×10^{9}	5.58×10^{10}	3.1×10^{12}	3.1×10^{9}
Maximum total erupted mass (*kg*)	1×10^{12}	5.58×10^{10}	5.52×10^{11}	3.1×10^{13}	3.1×10^{10}
Minimum column height *(m a.s.l.)*	10,000	3,000	11,000	26,000	2,000
Maximum column height (*m a.s.l.*)	20,000	11,000	20,000	35,000	8,000
Duration (*hours*)	-	1–4	2–6	2–6	1–2
Wind					
Number of wind files	14608	14608	14608	14608	14608
Wind start	01-Jan-2005	01-Jan-2005	01-Jan-2005	01-Jan-2005	01-Jan-2005
Winds per day	4	4	4	4	4
Grain Size Distribution					
Grain size *(φ)*	–6–6	–6–6	–6–7	–6–7	–3–7
Median phi *(φ)*	–1–2	–1–2	–1–2	–1–2	–0.5–3
Standard deviation *(φ)*	1–2	1–2	1–2	1–2	1.5 - 2.5
Tephra2 model					
Eddy constant *(m^2s^{-1})*	0.04	0.04	0.04	0.04	0.04
Diffusion Coefficient *(m^2s^{-1})*	100–10,000	1000	7000	7000	1000
Fall time threshold *(s)*	100–10,000	100	5000	10000	100
Lithic density *($kg\ m^{-3}$)*	2400	2600	2600	2600	2600
Pumice density *($kg\ m^{-3}$)*	400	400	400	400	400
Integration steps	60	100	100	100	100
Alpha (α)	1–4	3	3	3	3
Beta (β)	0.01–4	1.5	1.5	1.5	1.5

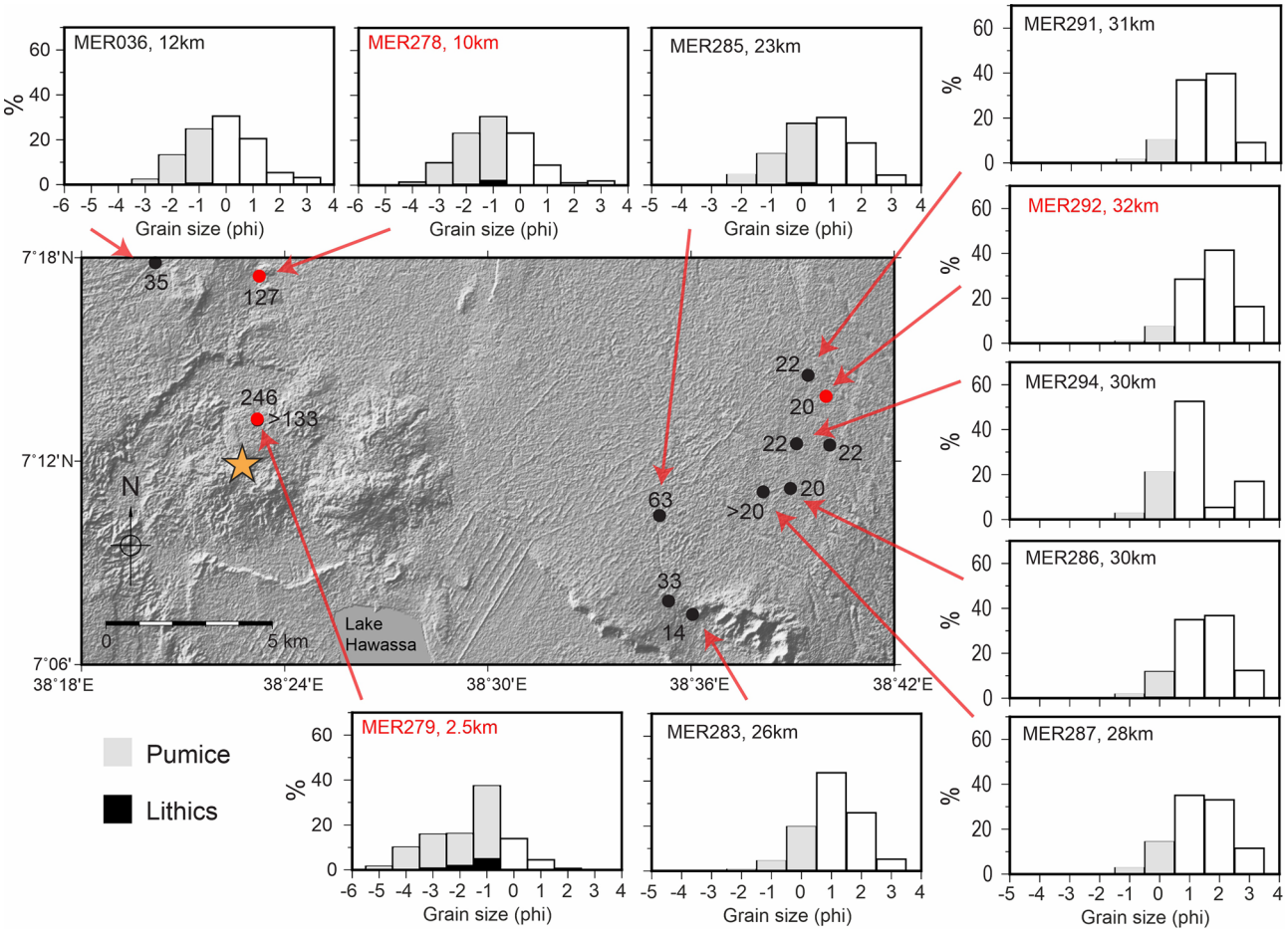


Fig. 5 Map showing thickness (cm) and grain size distributions of the WKYP deposit at various distances from the volcano. The locations in red are those shown in fig. 3. The eruption source is indicated by the star. Clasts greater than −1 phi (2 mm) in size were separated into pumice and lithic components. Background map: NASA/METI/AIST/Japan Spacesystems and U.S./Japan ASTER Science Team (2009)

phi. We chose to set the fine grain size limit at 7 phi as it is assumed that finer material would fall either as aggregates captured within these grain size bounds or be dispersed much further than the tephra fall footprints being simulated.

Phreatomagmatic eruptions are typically fine-grained reflecting the high fragmentation efficiency caused by magma interactions with external water (Cashman and Rust 2016). For our phreatomagmatic scenario, we have therefore chosen a grain size distribution reflective of this, using data from the Grímsvötn 2004 basaltic phreatomagmatic eruption (Jude-Eton et al. 2012; Gudmundsdóttir et al. 2016). Based on tectonic setting and geochemistry, we consider Icelandic volcanoes suitable analogues to Ethiopian volcanoes (Tierz et al. 2019). Although the eruption was mafic and erupted through an ice cap, the total grain size distribution (TGSD) of the Grímsvötn 2004 eruption is within the range generated by other Iceland volcanic eruptions of more intermediate compositions (e.g., Katla volcano; Gudmundsdóttir et al. 2016) and is consistent with suggested values for dispersion modelling provided by Cashman and Rust (2016). In addition, the Grímsvötn 2004 TGSD is close to the average derived by Michaud-Dubuy et al. (2025) from twelve TGSDs compiled in the IVESPA database (Aubry et al. 2021) for phreatic and phreatomagmatic eruptions.

Particle Density: Pumice from Corbetti deposits are similar in composition to trachytic pumice clasts from Rungwe which have densities of 400–450 kg m^{-3} (Fontijn et al. 2011). Pumice clasts at Corbetti are highly vesicular, with abundant tube pumice observed. Highly inflated clasts are also observed within the Corbetti tephra deposits, and the deposits are generally lithic poor (Fig. 5). The deposit density is therefore assumed not much higher than the pumice density, with 90:10 pumice to lithic ratio. The average bulk deposit density is assumed to be 620 kg m^{-3} (validated with the expert group), based on a pumice density of 400 kg m^{-3} and lithic density of 2600 kg m^{-3}.

Total erupted mass: Volumes following the volcanic explosivity index (VEI) are applied here: the total erupted mass ranges were calculated from the volume ranges and bulk density (620 kg m^{-3}). The VEI classification includes

all pyroclastic fall and flow material. A VEI 4 event would likely produce pyroclastic density currents; therefore, we assume 90% of pyroclastic material would be dispersed as tephra within an eruption plume (e.g., Calbuco 2015 eruption; Romero et al. 2016). A VEI 6 caldera forming eruption would likely result in significant pyroclastic density currents; therefore, we assume the tephra fallout to comprise 50% of the total erupted volume. However, we acknowledge that the partitioning between buoyant plumes and PDCs can be highly variable (e.g. Carazzo et al. 2015), which would influence the tephra fall footprints.

Eruption Column Height: The minimum and maximum eruption column heights were calculated from the above erupted masses based on the empirical relationship derived by Jenkins et al. (2007) for explosive events:

$$\text{Height (km asl)} = 8.67 \times \log_{10}(\text{Volume in km}^3) + 20.2$$

The relationship assumes a sustained plume with no effect from wind on the plume height, therefore only works for larger magnitude eruptions, or low wind scenarios. For a lower volume VEI 3 event, an eruption column height range consistent with the VEI classification was selected.

Phreatomagmatic eruptions tend to have lower column heights than their magmatic equivalents (in terms of mass eruption rate) due to the loss of thermal energy turning water to steam (Cole et al. 1995). The IVESPA database compiled 37 phreatic and phreatomagmatic eruptions ranging in plume height from 2.3 to 17.5 km a.s.l (Aubry et al. 2021; Michaud-Dubuy et al. 2025). Observed phreatomagmatic PDC deposit runout lengths from a tuff ring at Corbetti volcanic system are approximately 6 km (Ben Clarke, personal communication, 2018). Column heights of 6–10 km a.s.l. were reported from the phreatomagmatic Grímsvötn 2004 eruption (Jude-Eton et al. 2012). Therefore, we consider it reasonable to assume a column height of between 2 and 8 km a.s.l. for a VEI 2 to 3 phreatomagmatic event.

Plume model: The alpha and beta parameters describe the mass distribution of tephra within the plume: if $\alpha=\beta=1$, then particles are dispersed uniformly within the plume; if $\alpha>\beta$, then particles are released from the top part of the plume; if $\alpha<\beta$, then particles are released from the bottom part of the plume. We have selected α and β values of 3 and 1.5 respectively for all scenarios, consistent with our *Tephra2* inversion modelling results and other studies (e.g., Yang et al. 2021; Jenkins et al. 2022).

Diffusion coefficient and fall time threshold: These parameters describe the diffusion of particles as they fall through the plume and atmosphere. The diffusion coefficient accounts for the horizontal diffusion of large particles: the larger the diffusion coefficient the more widespread the plume. The fall time threshold accounts for change in diffusion law based on total particle fall time, allowing fine particles to fall out. Values for the scenarios modelled in *TephraProb* were selected based on the inversion modelling results.

Event duration: *Tephra2* assumes that the input parameters are representative for the average conditions over the peak eruption duration, and that most tephra is ejected in a short duration (few hours) explosive event (Connor and Connor 2006). *TephraProb* however, requires a duration input value. For a VEI 3 event (scenario 1), we assume a duration of 1 to 4 hours (1 is the minimum value possible), for a larger magnitude VEI 4 and 6 event, we assume a duration of between 2 and 6 hours, and for a low magnitude event we assume a duration of 1 to 2 hours.

Wind: *Tephra2* uses NOAA-NCEP Reanalysis2 wind data (NOAA 2015). To account for variations in wind conditions, ten years of wind data for Corbetti were downloaded from 1st January 2005 to 31st December 2014, for 17 wind levels from approximately 150 to 30,000 m a.s.l. We ran 1000 simulations for a dataset of wind over ten years, sampled 4 times daily (14,608 files). We assume that current weather conditions are representative of past conditions; however, acknowledge the uncertainty associated with this assumption.

TephraProb uses the European Centre for Medium-Range Weather Forecasts (ECMWF) ERA-Interim global reanalysis dataset (Dee et al. 2011). We used a ten-year dataset from 1st January 2005 to 31st December 2014, sampled four-times daily (14,608 wind files) to account for variations in wind conditions that could impact the tephra fall footprint (Fig. 6).

Various combinations of input parameters can match the observed deposit thickness and grain size data (Connor and Connor 2006; Scollo et al. 2008). To account for this, *Tephra2* uses the downhill simplex algorithm (Nelder and Mead 1965; Connor and Connor 2006), a non-linear inversion model run in parallel on multiple processors, to search for the best-fit eruption parameter set that minimises the error between the measured tephra thickness and grain size distribution, and the model outputs (Connor and Connor 2006). As well as uncertainties related to the data and input parameters, there are uncertainties related to the numerical model itself. For example, due to the complexities involved in modelling atmospheric conditions, *Tephra2* does not consider horizontal changes in wind conditions away from the vent. Several assumptions are made on diffusion and particle fallout, which will be different for each explosive event depending on atmospheric conditions, mass eruption rate, particle size and particle density (Connor and Connor 2006). For detailed discussion on tephra dispersion modelling uncertainties, the reader is referred to Scollo et al. (2008). For more details on uncertainties related to tephra dispersion models the reader is referred to Scollo et al. (2008) and Bonadonna et al. (2015).

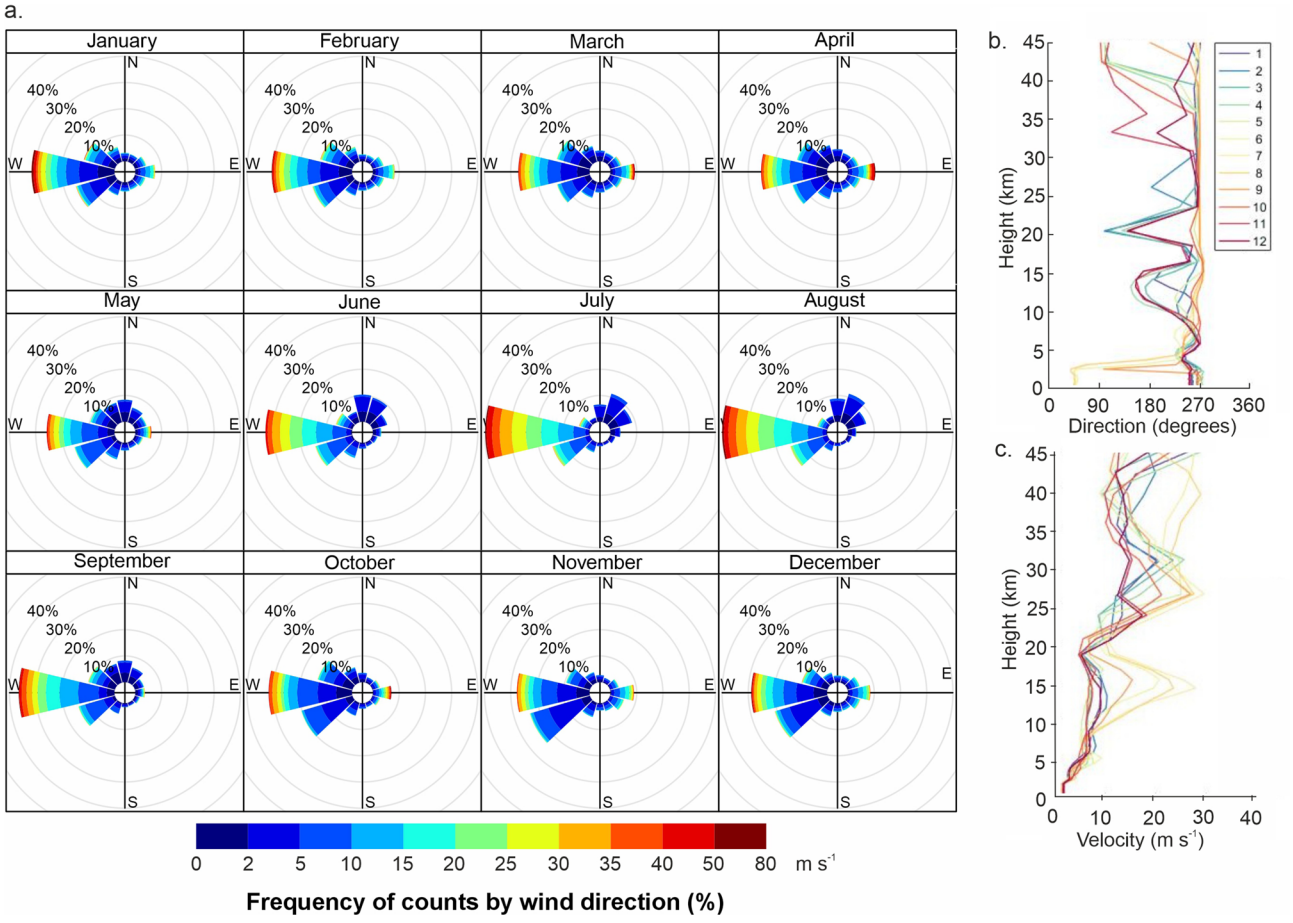


Fig. 6 Ten-year ECMWF ERA-interim global reanalysis (Dee et al. 2011) dataset for Corbetti from 1st January 2005 to 31st December 2014, separated by month to show seasonal variation in wind direction. a. Wind roses with coloured bars showing the direction the wind is blowing, colours represent the wind speed, and the length of the bar represents the frequency of counts by wind direction (%). b. Vertical profile of wind direction with height by month. c. Vertical profile of wind velocity with height by month

Exposure analysis

To analyse exposure to tephra fall, we used the open access *VolcGIS* Python package (Biass et al. 2022a). *VolcGIS* was developed to integrate volcanic hazard footprint maps with open access global exposure data, which include population, land cover and road networks (Jenkins et al. 2022). *VolcGIS* pre-processes the hazard output files (readable ASCII rasters) and exposure data sets to unify them in one grid of the same projection as the target volcano (Jenkins et al. 2022). Once the files have consistent geographic references (including coordinate system, extent, resolution and pixel count), the exposure for the exceedance probability (10 and 50%) for each class of tephra load threshold (i.e. 1, 10, 100 kg m^{-2}) can be calculated.

To consider exposure around the Corbetti volcanic system, LandScan 2019 global population, Copernicus global land cover and OpenStreetMap geographic data were used. LandScan 2019 Global population data is generated using census counts and high-resolution remote-sensing imagery to provide an estimated population count for each cell at 30-arcsecond grid resolution (approximately 1 km; Rose et al. 2020). Exposure was calculated for 10, 30, 50 and 100 km radius from the Corbetti volcanic system (Uriji vent) and tephra fall footprints. Following Jenkins et al. (2022), the Copernicus Global Land Cover v3 at 100 m resolution (CGLS-LC100; Buchhorn et al. 2020) for 2019 was used to estimate exposure of crops and urban areas to tephra fall.

OpenStreetMap (http://openstreetmap.org/copyright) provides global geographic data including transport infrastructure, buildings, points of interest, natural features, and land use data. OpenStreetMap relies on members across the globe to map features, therefore, data quality and accuracy can be variable. Geofabrik is a member of OpenStreetMap and provide free data available to download from their website. The shapefiles are automatically updated daily. Data for this research were downloaded from Geofabrik on 26th August 2022.

Table 3 Recurrence rate in years of any explosive eruption, and VEI 3 (explosive Vulcanian) and VEI 4 (sub-Plinian to Plinian) explosive events at Corbetti volcanic system derived from expert elicitation

	Any eruption	VEI 3 (Vulcanian)	VEI 4 (Sub-Plinian to Plinian)
25th percentile	400	388	3,040
Median	**520**	**1,152**	**13,109**
75th percentile	909	5,692	77,467

Results

Expert elicitation

The group consensus on the median recurrence rate for any explosive silicic eruption at Corbetti volcanic system was 520 years, giving an annual eruption probability (approximate inverse of recurrence rate) of 0.0019 (Table 3).

Low-moderate volume 'explosive Vulcanian' (VEI 3) type pumice cone forming eruptions were considered 10 times more likely than moderate to large magnitude 'sub-Plinian' to 'Plinian' (VEI 4) eruptions. The 75th confidence interval show the high level of uncertainty among the experts, especially towards the upper limits for a VEI 4 event (Table 3).

Tephra hazard analysis

Inversion modelling of WKYP pumice

Probabilistic inversion modelling of the WKYP deposit reveals a median eruption column height of 16 km a.s.l. and a median erupted mass of 8.7×10^{11} kg for the top 100 best fit results (out of 1000). The best fit wind data gives an eruption column height of 18 km a.s.l. and an erupted mass of 8.4×10^{11} kg (Supplementary data), or 1.3 km^3 assuming an average bulk deposit density of 620 kg m^{-3}. These results are consistent with the volume estimate of Fontijn et al. (2018).

The tephra dispersion map generated using the best fit input parameters from the inversion modelling for the WKYP eruption, reveals tephra deposition to the east with a tephra fall load of approximately 200 kg m^{-2} in the town of Shashemene, equivalent to a thickness of approximately 30 cm assuming a bulk deposit density of 620 kg m^{-3} (Fig. 7).

Probabilistic tephra fall hazard analysis

Probabilistic tephra dispersion maps are presented in Figs. 8 to 11 for each eruption scenario, for tephra accumulation thresholds of 1, 10 and 100 kg m^{-2}, which correspond to approximately 1.6 mm, 16 mm and 16 cm,

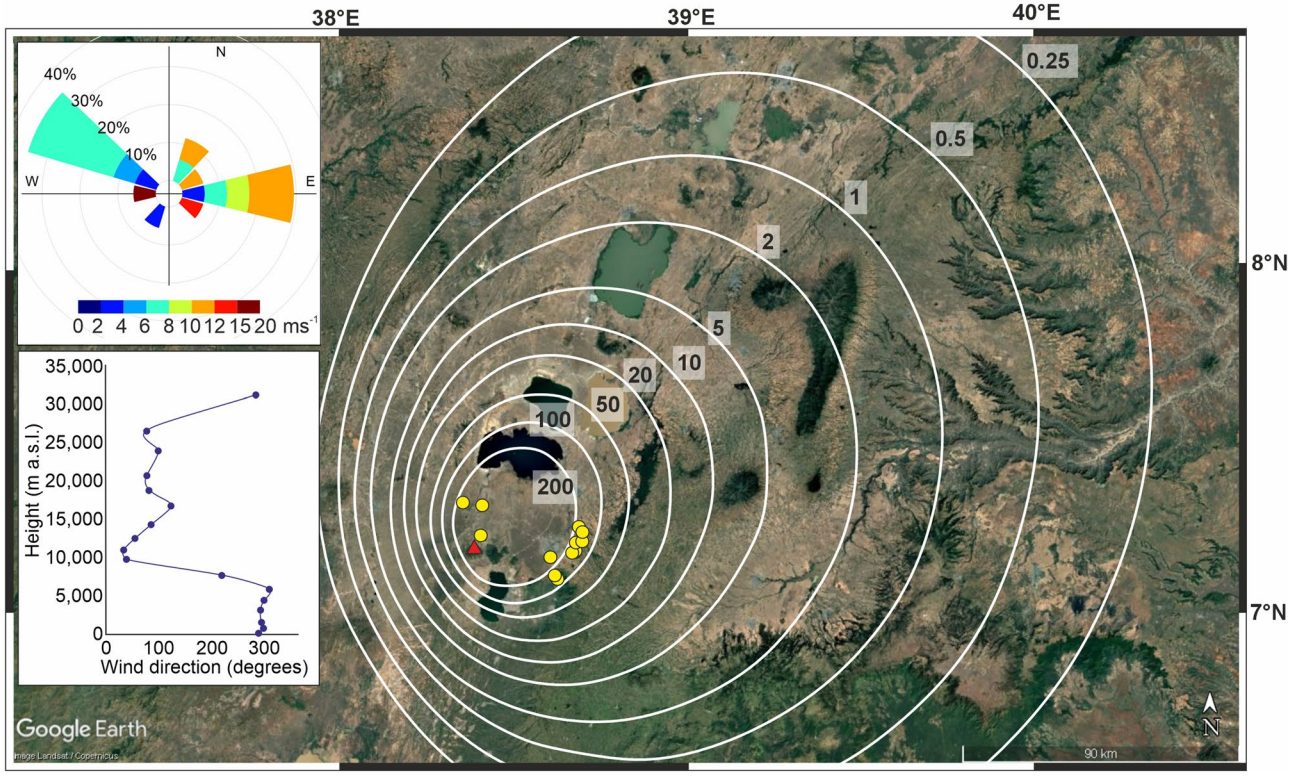


Fig. 7 Tephra dispersion map of the WKYP deposit output from the *Tephra2* forward model using the best fit inversion parameters to replicate the dispersion of the WKYP tephra deposit. Isomass contours show the tephra load, from 0.25 kg m^{-2} to 200 kg m^{-2}. Yellow dots show sample locations. The inserts show the rose diagram for the best fit wind profile, with coloured bars representing the direction the wind is blowing to and wind speed, and the vertical profile of the wind direction with height (m a.S.l.). Basemap: Google Earth © 2025 Maxar Technologies/Airbus/CNES/Airbus

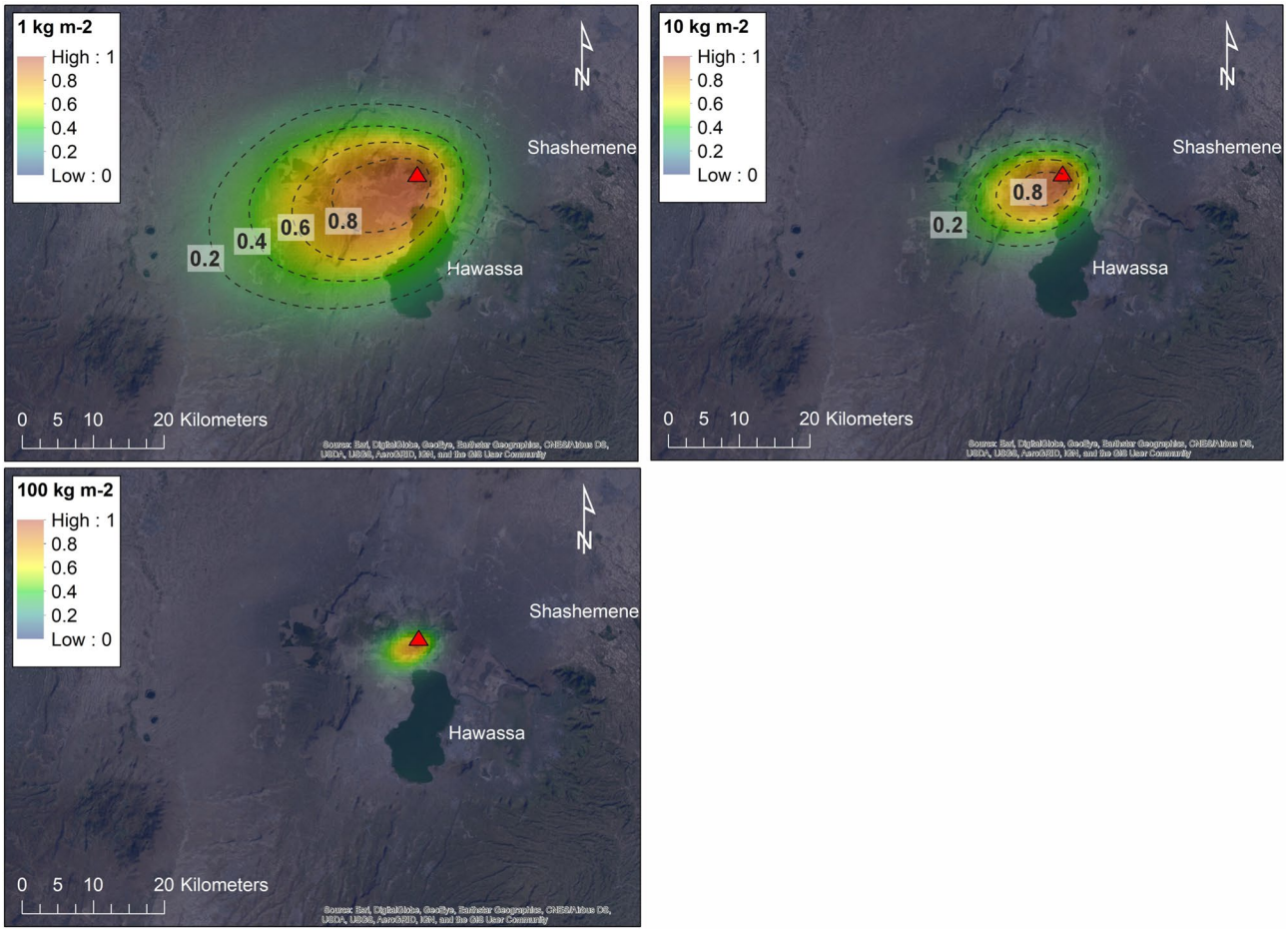


Fig. 8 Probability of tephra accumulation exceeding 1, 10 and 100 kg m^{-2} (~1.6 mm, 16 mm and 16 cm, respectively) for scenario 1: a low-to-moderate volume silicic explosive event (VEI 3; eruption column height 3–11 km a.s.l.). The vent is shown by the triangle. Basemap: ESRI world imagery (sources: Esri, Maxar, earthstar geographics, and the GIS user community)

respectively, assuming an average bulk deposit density of 620 kg m^{-3}. The tephra accumulation threshold of 250 kg m^{-2} is also included in Figs. 9 and 10 (VEI 4 and 6 scenarios), corresponding to approximately 40 cm thickness. The maps show the probability of exceeding the selected tephra accumulation threshold for each scenario. Given the plume heights considered, it is not anticipated that the size or shape of the dispersal area would change significantly if the vent location was changed, but the impacted areas would change accordingly.

Results reveal tephra dispersion towards the west for all scenarios reflecting the dominant wind direction (as observed in Fig. 6). Results for Scenario 1, a low-to-moderate explosive event (VEI 3), reveal high probabilities (~0.8) of tephra accumulation exceeding 1 kg m^{-2} (~1.6 mm thickness) at distances of up to 15 km from the vent (Fig. 8). For tephra loads exceeding 100 kg m^{-2} (~16 cm thickness), the probability is very low (~0.1) beyond 10 km of the vent. Within 5 km of the vent, the probability increases to 0.6, with a high probability of >100 kg m^{-2} (~16 cm) of tephra fall within 1–2 km of the vent.

Results for Scenario 2, a large volume explosive event (VEI 4), indicate high probabilities (0.7–0.8) of tephra loads exceeding 1 kg m^{-2} (~1.6 mm) within 30 km downwind of the vent (Fig. 9). The probability of exceeding 100 kg m^{-2} (~16 cm), is very high (>0.8) within 10 km of the vent. Exceedance probabilities for 250 kg m^{-2}, corresponding to approximately 40 cm of tephra thickness, also highlight substantial loading with a 0.5 probability of exceeding this threshold within 10 km downwind of the vent (Fig. 9).

Results for Scenario 3, a VEI 6 large magnitude caldera-forming event, reveal widespread tephra dispersion (Fig. 10). Even probabilities of tephra loads greater than 250 kg m^{-2} (~40 cm thickness) are high (~0.8) within 30 km downwind of the vent.

An off-edifice low-volume phreatomagmatic event close to the northern shore of Lake Hawassa (Scenario 4), would likely result in localised tephra dispersal, with less than 0.2 probability of over 1 kg m^{-2} (~1.6 mm)

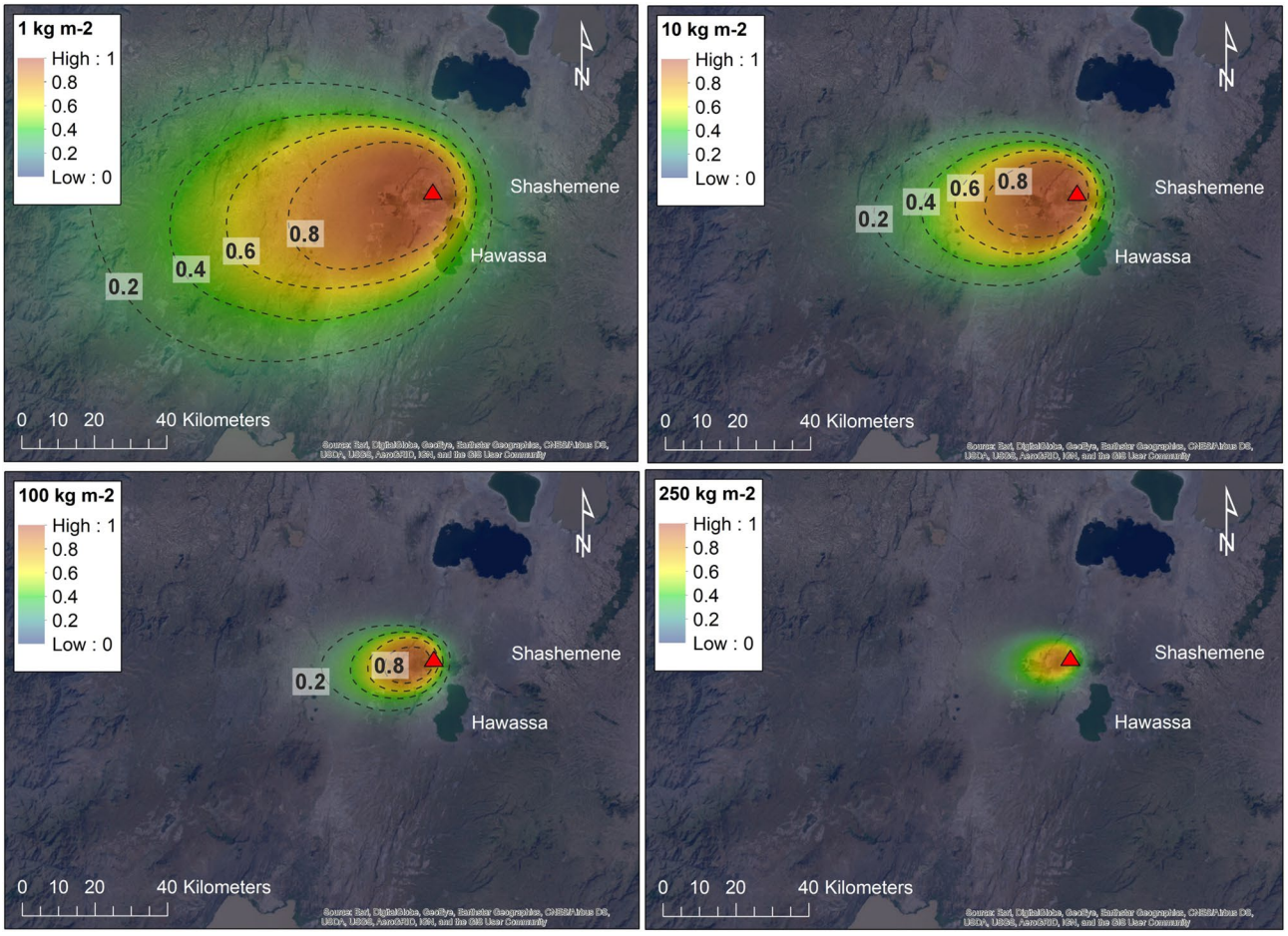


Fig. 9 Probability of tephra accumulation exceeding 1, 10, 100 and 250 kg m^{-2} for scenario 2: a large volume explosive silicic explosive event (VEI 4; eruption column height 11–20 km a.s.l.). Equivalent thicknesses are 1.6 mm, 16 mm, 16 cm and 40 cm, respectively. The vent is shown by the triangle. Basemap: ESRI world imagery (sources: Esri, Maxar, earthstar geographics, and the GIS user community)

accumulation within 20 km of the vent (Fig. 11). Results reveal very low (<0.1) probabilities of exceeding 10 kg m^{-2} (~16 mm) of tephra accumulation beyond 10 km from the vent.

Exposure

Ethiopia has a population of approximately 105 million (Ethiopian Statistical Service 2023), with the most densely populated areas along the rift margins or in the rift valley (Fig. 12).

Analysis of the LandScan global population dataset using VolcGIS reveals ~40,000 people living within 10 km of the central vent, more than 3.6 million people living within a 50 km radius of the central vent, and over 12.6 million people living within a 100 km radius of the central vent (Table 4).

Integration of the probabilistic tephra fall maps with exposure data (Table 5; Fig. 13) reveals the potential for over 47,000 people to be impacted by 1 kg m^{-2} (~1.6 mm thickness) tephra fall (50% exceedance probability) from a low-moderate volume VEI 3 event (Table 5; Fig. 13 a,b). Over 2000 people could be impacted by over 100 kg m^{-2} (~16 cm thickness) of tephra fall from the same event. For a moderate to large volume VEI 4 event (Fig. 13 c,d), over 770,000 people and over 3000 km of roads have the potential to be impacted by 1 kg m^{-2} (~1.6 mm thickness) of tephra fall. For a VEI 6 event (Fig. 13 e,f), over 12 million people have the potential to be impacted by 1 kg m^2 and just over 985,000 people could be impacted by 100 kg m^{-2} (~16 cm thickness) of tephra fall (Table 5).

For scenario 4, an off-edifice low volume phreatomagmatic event (Fig. 13 g,h), tephra loads of over 1 kg m^{-2} (~1.6 mm) could impact significant numbers of people (approximately 29,000), crop cover (77 km^2) and roads (247 km), as well as the airport and geothermal infrastructure (Fig. 13 g).

Discussion

Recurrence intervals of future explosive events

The most recent explosive eruptions at the Corbetti volcanic system have been dated at 1.3–0.5 ka, based on tephra from lake cores (Martin-Jones et al. 2017), and

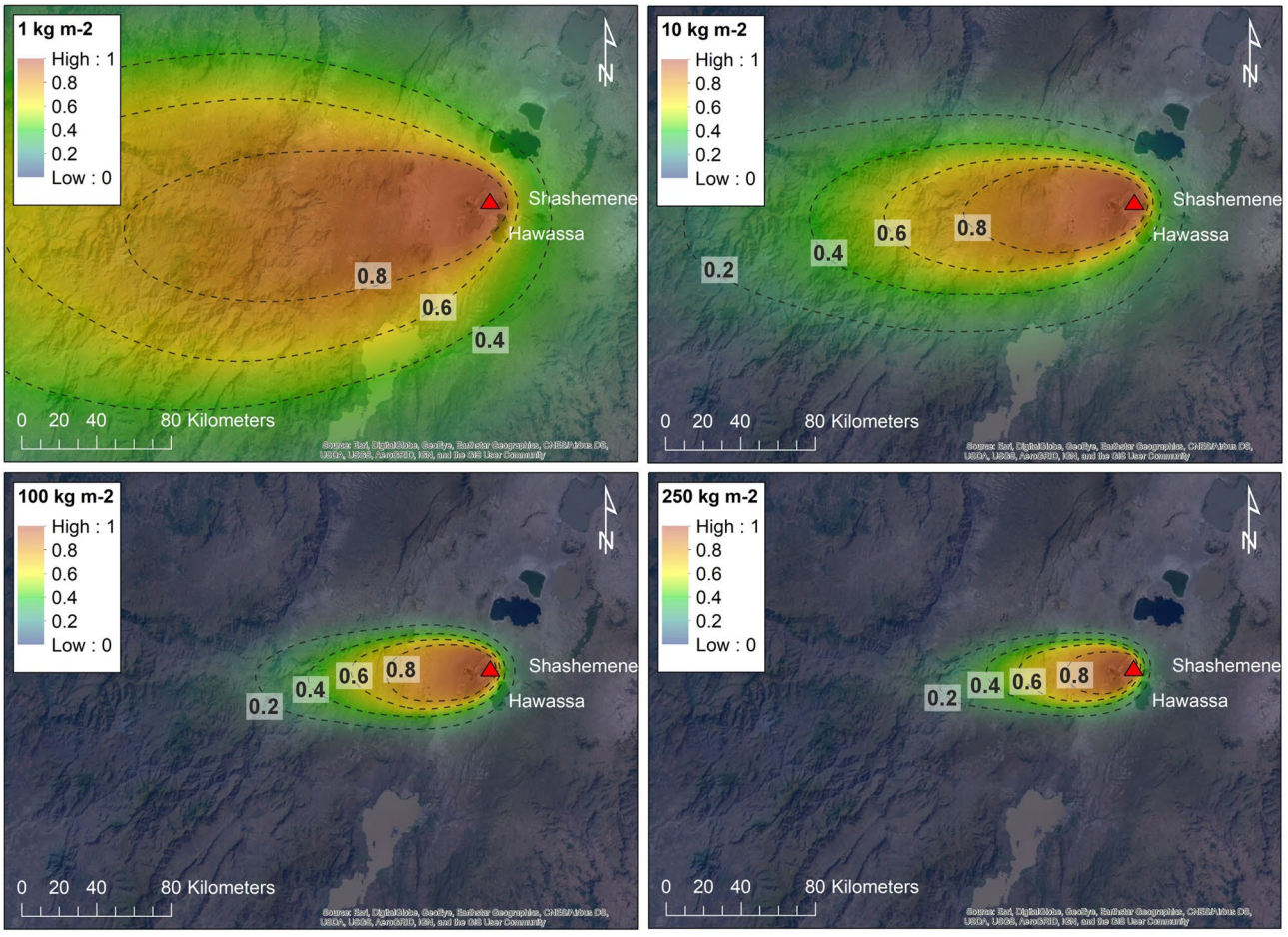


Fig. 10 Probability of tephra accumulation exceeding 1, 10, 100 and 250 kg m^{-2} for scenario 3: a large volume caldera forming explosive event (VEI 6; eruption column height 26–35 km a.s.l.). Equivalent thicknesses are 1.6 mm, 16 mm, 16 cm and 40 cm, respectively. The vent is shown by the triangle. Basemap: ESRI world imagery (sources: Esri, Maxar, earthstar geographics, and the GIS user community)

approximately 2.3 ka for the WKYP deposit (Rapprich et al. 2016). Drawing on these studies and additional data collected during the RiftVolc project, our expert elicitation yielded an average recurrence interval of 520 years for any silicic explosive event, with 25th and 75th percentiles of 400 and 909 years, respectively. These values are broadly consistent with previous estimates of 700–1000 years (Fontijn et al. 2018) and 900 years (Martin-Jones et al. 2017), which fall within the elicitation uncertainty range.

Jenkins et al. (2024a) reported average recurrence intervals for eruptions at Corbetti across several VEI categories. Their expert elicitation was conducted in 2015, prior to the RiftVolc project (2014–2021) and other studies that advanced understanding of volcanic activity at Corbetti. Consequently, eruption history and future explosive event scenarios were derived using analogue volcanoes. Comparing those results with this study shows that our estimates indicate a higher average recurrence interval for any VEI and for VEI 3 events, but with substantially narrower uncertainty bounds (Table 6). VEI 4 events, which were considered much less likely in this study, yielded an average recurrence interval of 13,109 years compared to 3,600 years in Jenkins et al. (2024a); however, both estimates remain subject to considerable uncertainty. This suggests that improved knowledge of eruptive history has enabled better constraints on average recurrence intervals and associated uncertainties for any explosive event, and lower-magnitude VEI 3 events. However, the results for VEI 4 explosive events likely reflect a high level of uncertainty among experts regarding the occurrence of larger-magnitude eruptions at this central rift volcano. Much of the elicitation discussion focused on the preservation of deposits and the completeness of terrestrial and lake records (Crummy et al. 2018), as well as the different eruption styles observed in the past or anticipated in the future. Because the elicitation was conducted prior to the work of Colby et al. (2022) on Corbetti's eruptive history, a future elicitation incorporating this knowledge may provide better constraints on uncertainties surrounding highly explosive events.

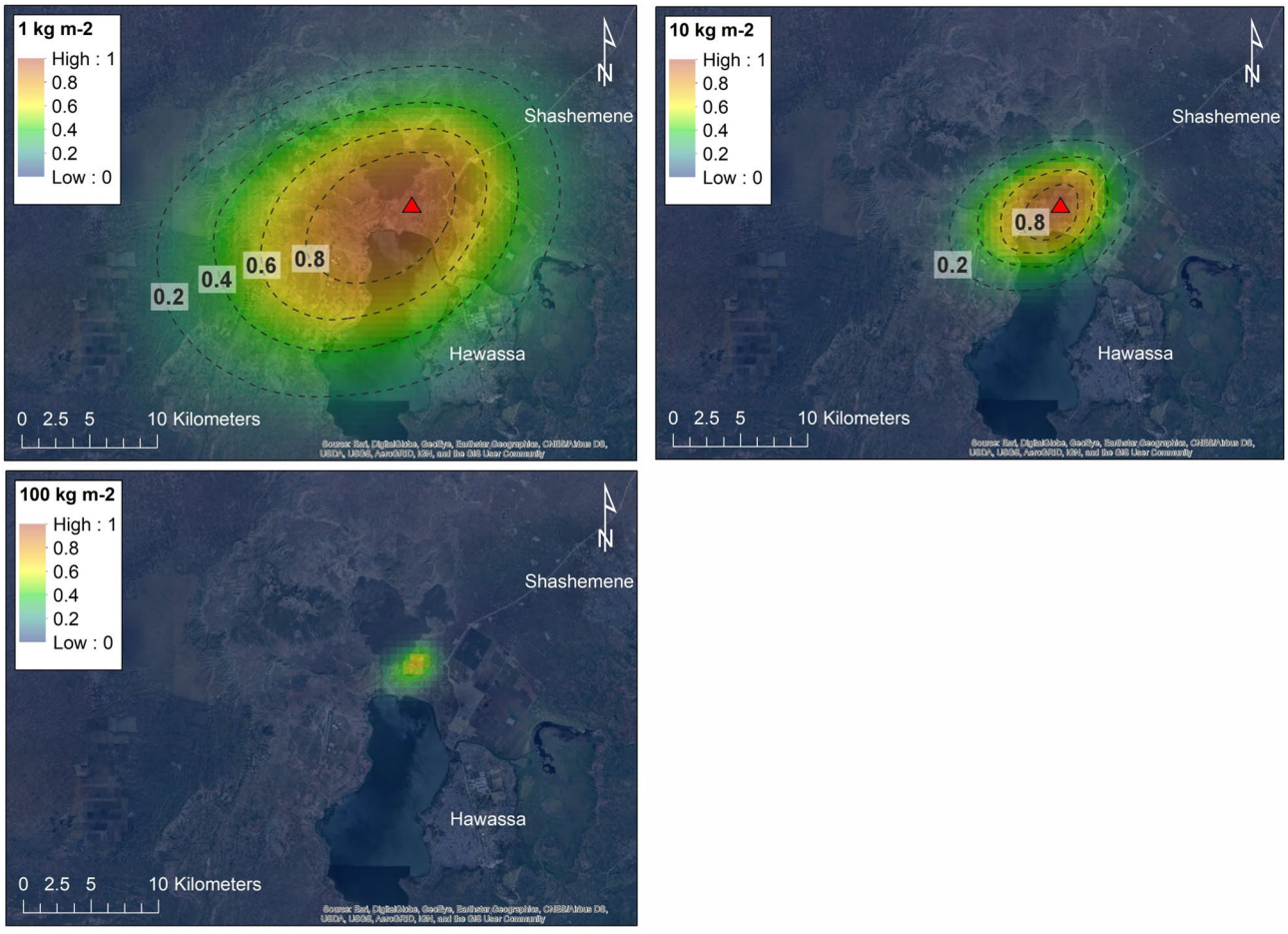


Fig. 11 Probability of tephra accumulation exceeding 1, 10 and 100 kg m^{-2} (~1.6 mm, 16 mm and 16 cm, respectively) for scenario 4: an off-edifice phreatomagmatic VEI 2 to 3 explosive event (eruption column height 2–8 km a.s.l.). The vent is shown by the triangle. Basemap: ESRI world imagery (sources: Esri, Maxar, earthstar geographics, and the GIS user community)

Tephra fall footprints

Field data and inversion modelling of the WKYP deposit reveal tephra dispersion predominantly towards the east, with load contours displaying a rounded shape (Fig. 6). Mass eruption rate can influence the dispersal of tephra and resultant tephra fall footprints (Bonadonna and Costa 2013). *Tephra2* accounts for this by exploring variations in mass eruption rate based on ranges of total erupted mass, eruption column heights, duration and wind conditions (Biass et al. 2016). Tephra dispersal is also strongly influenced by plume dynamics and atmospheric conditions (Bonadonna and Costa 2013). For example, weak plumes under calm conditions may produce circular fallout patterns (e.g., Ruapehu 1996 eruption; Bonadonna et al. 2005b), where as weak to moderate plumes in strong winds can result in elongated dispersal (e.g., Eyjafjallajökull 2010 eruption; Bonadonna et al. 2011; Stevenson et al. 2012). The wind data for the best fit inversion parameters show the winds blowing predominantly to the west at lower altitudes (up to ~ 7500 m a.s.l.) and to the east at mid altitudes, ~9000 to 25,000 m a.s.l. (Fig. 7), giving the contours their rounded shape. However, there is significant uncertainty associated with this, for example, we assume that present wind patterns approximate those of the late Holocene. Furthermore, sample locations are relatively proximal (<30 km) and concentrated to the north and east, providing limited constraint on distal dispersal. Notably, Martin-Jones et al. (2017) identified a WKYP tephra layer in Lake Tilo, 40 km west of Corbetti. Additional targeted fieldwork to the south and west could improve constraints on the extent and complexity of this deposit.

In contrast to the WKYP deposit, probabilistic tephra dispersion modelling of the four scenarios reveals that the majority of tephra is dispersed towards the west of the volcano. The maps are generated by summing the separate simulations ($n = 1000$) and calculating the probability for a wide range of tephra accumulations at each pixel, therefore they reflect the predominant wind direction (Fig. 6). However, there are variations in wind direction with height, and during different months of the year. While the probabilistic maps reveal predominant tephra

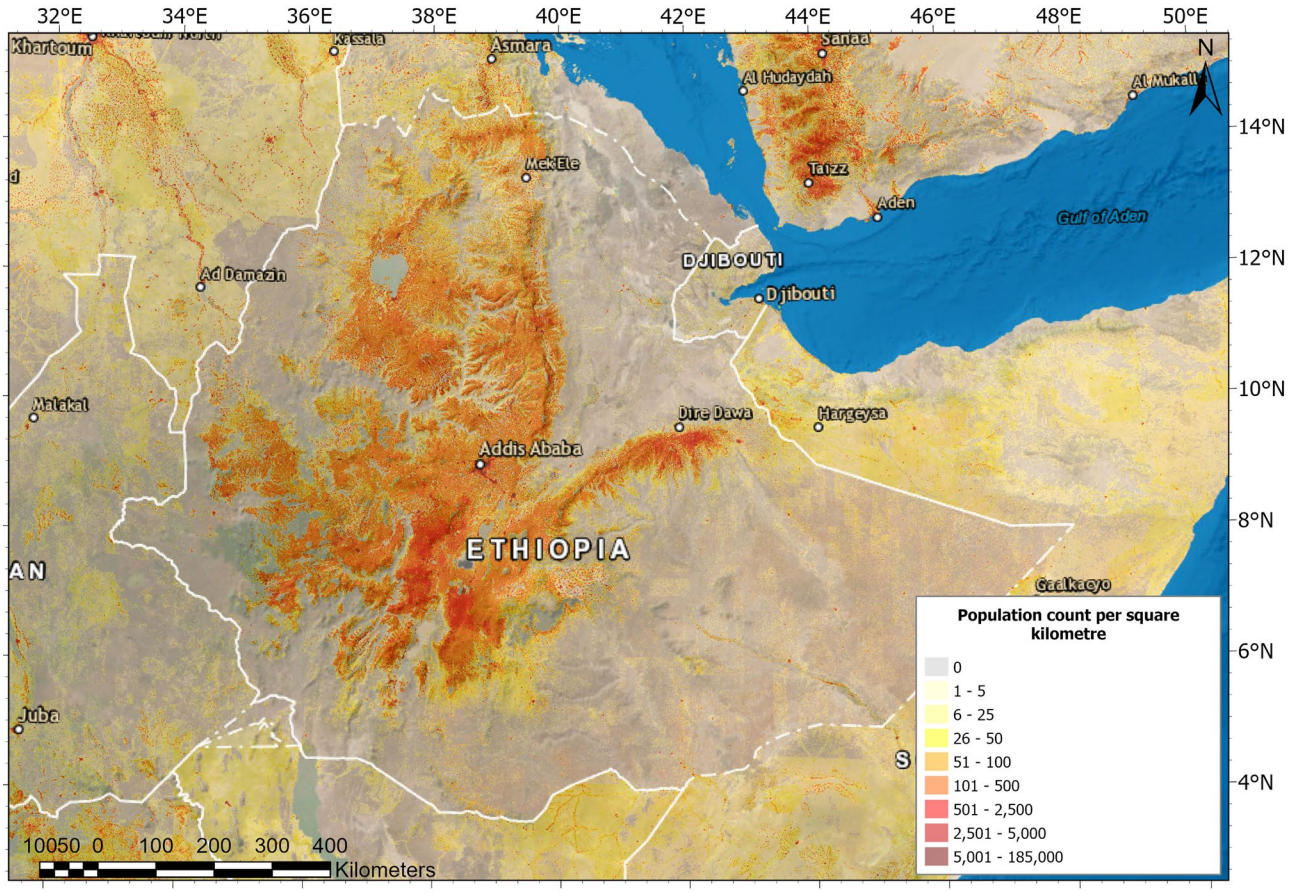


Fig. 12 LandScan 2019 Global estimated population count per square kilometre (Rose et al. 2020) for Ethiopia. Darkest red areas have the highest population density. Basemap: ESRI world imagery (sources: Esri, Maxar, earthstar geographics, and the GIS user community)

Table 4 Estimated exposure within 10, 30, 50 and 100 km radius of the Corbetti central vent, incorporating LandScan 2019 global population (Rose et al. 2020), Copernicus global land cover (Buchhorn et al. 2020) and OpenStreetMap geographic data (http://openstreetmap.org/copyright), derived using *VolcGIS*

	10 km	30 km	50 km	100 km
Population count	40,768	1,464,509	3,613,734	12,648,312
Crop cover (km^2)	171	2,131	849	1,861
Urban areas (km^2)	0	49	80	192
Primary roads (km)	0	187	318	999
Secondary roads (km)	33	549	1,522	4,734
Local roads (km)	331	5,477	9,871	26,333
Motorway (km)	0	0	0	35
Total roads (km)	365	6,213	11,711	32,101

dispersal to the west, individual eruptions will be influenced by the vertical wind, therefore will likely show more variation. For example, the averaged vertical wind profile for December from the reanalysis dataset (Fig. 6b) shows winds blowing towards the west at altitudes of 0 to ~ 9 km a.s.l. and towards the south at altitudes of ~ 9 to 16 km a.s.l. This implies that an eruption during December may result in tephra fall in communities to the south

Table 5 Estimated exposure to tephra fall thresholds of 1, 10 and 100 kg m^{-2} (~1.6 mm, 16 mm and 16 cm thickness; 50% exceedance probability) for each scenario. Estimated exposure for 10% exceedance probability are provided in Supplementary data

Scenario	Tephra mass (kg m^{-2})	Population count	Crop cover (km^2)	Urban area (km^2)	Roads (km)
1 (VEI 3)	1	47,535	146	0	412
	10	16,166	56	0	162
	100	2,036	10	0	42
2 (VEI 4)	1	777,226	1,677	7	3,399
	10	197,578	629	0	1,734
	100	37,071	135	0	499
3 (VEI 6)	1	12,043,761	1,049	172	6,507
	10	3,730,276	1,516	53	1,707
	100	985,683	1,707	16	523
4 (VEI 2/3)	1	29,097	77	0	247
	10	9,292	33	0	114
	100	2,635	8	0	56

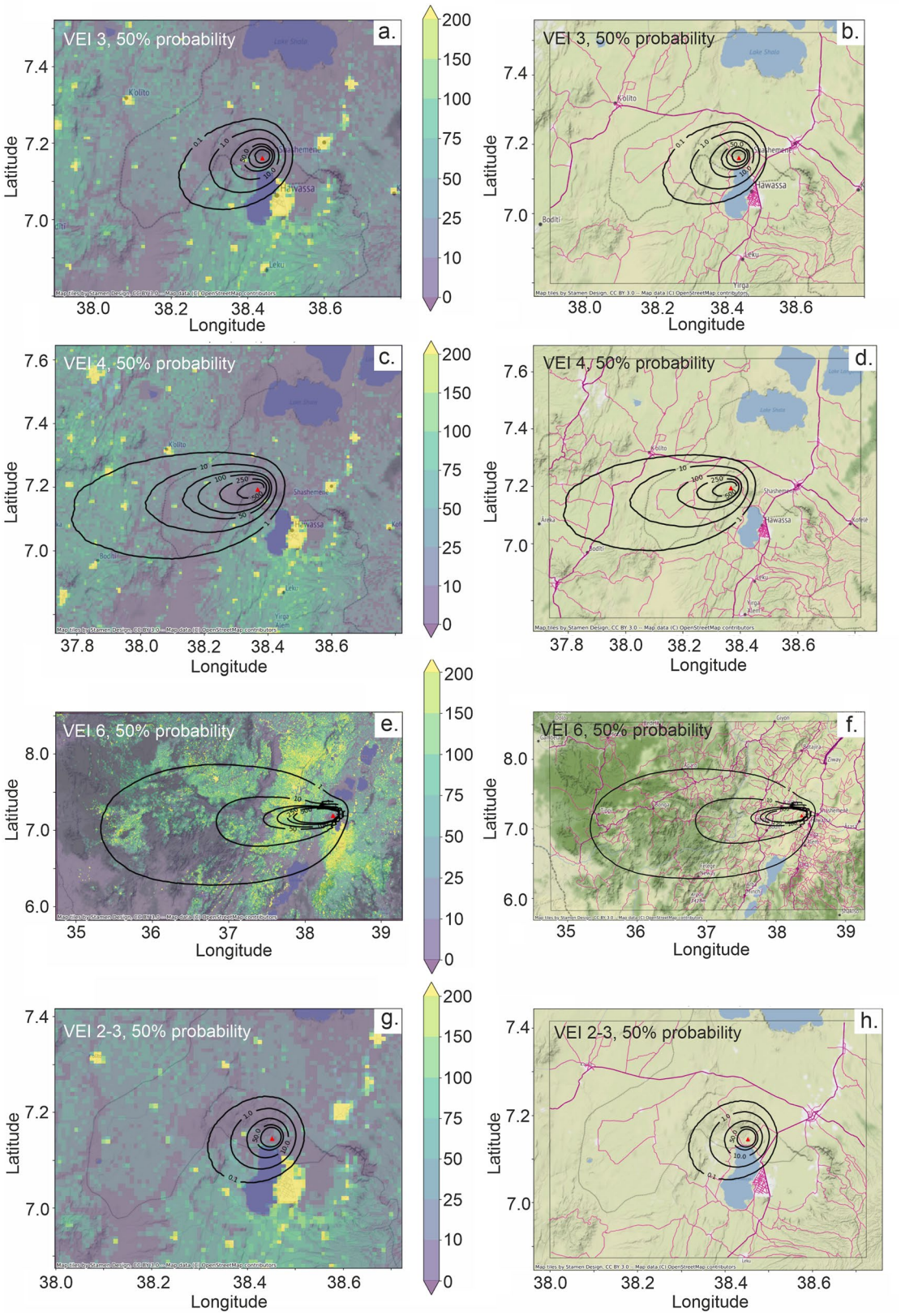


Fig. 13 LandScan 2019 Global population count per square kilometer (Rose et al. 2020) on left hand side, and OpenStreetMap roads (openstreetmap.Org/copyright) on right hand side overlain with 50% exceedance probability tephra loading contours (1, 10, 100, 250 and 500 kg m^{-2}) for a scenario 1 (VEI 3; a and b), scenario 2 (VEI 4; c and d), scenario 3 (VEI 6; e and f), and scenario 4 (VEI 2 to 3; g and h) event. Basemaps: ESRI world topographic map (sources: Esri, TomTom, Garmin, FAO, NOAA, USGS, © OpenStreetMap contributors, and the GIS user community)

Table 6 Elicited average recurrence intervals (median, with 25th – 75th percentile range in brackets) for any VEI, VEI 3 and VEI 4 explosive events from Jenkins et al. (2024a) and this study. *results from Colby et al. (2022), Fontijn et al. (2018) and Martin-Jones at al. (2017) derived from field evidence included for comparison

	Any VEI	VEI 3	VEI 4
This study	520 (400–909)	1152 (388–5692)	13,109 (3040–77,467)
Jenkins et al. (2024a)	308 (75–5000)	950 (515–15,500)	3600 (1950–58,000)
Colby et al. (2022)	300–400*		
Fontijn et al. (2018)	700–1000*		
Martin-Jones et al. (2017)	900		

and southwest of Corbetti, in the direction of Hawassa airport, assuming similar wind conditions today.

The tephra fall footprints present probabilistic outputs for possible future explosive scenarios based on all the available evidence, but should not be considered operational hazard maps. A future explosive event is unlikely to have the same source parameters and wind conditions modelled here; therefore, resultant tephra fallout could be very different to the maps presented in this study. These footprints are intended to demonstrate the potential dispersion and fallout of tephra from an explosive event to help inform future planning and decision-making in the Corbetti region.

Exposure to tephra fall

Integration of exposure data with tephra fall maps show that significant numbers of people could be exposed to a future explosive event at Corbetti volcanic system. With an estimated 14,000 people and the location of the Corbetti geothermal site within the caldera, even a low-magnitude eruption could have significant social, physical and economic impacts. For example, volcanic ash thicknesses of just 1–10 mm can cause transport problems (traction on roads and visibility), damage to electrical and mechanical components, blockages and clogging of water intake structures and infiltration systems, and irritation of eyes and airways (Table 1; Jenkins et al. 2015). Clean-up operations are usually localised with sweeping of roads and pavements and clearing of gutters and roofs; however, there can be a high demand for water for clean-up which can last for months if wind-remobilised tephra needs dampening (Jenkins et al. 2015; Hayes et al. 2019a). There are also health impacts that should be considered, especially in arid areas where ash fall deposits may linger for years and be remobilised by human activities (Horwell and Baxter 2006). In a recent study, Jenkins et al. (2024b) observed the ingression of fine volcanic ash into buildings through openings. These included windows, gaps around doors and windows, and ventilation gaps between the external walls and roof to allow air flow. This can also be an issue with wind remobilised ash, particularly in dry environments.

A larger volume, VEI 4 event, similar to the WKYP eruption, was considered less likely than a VEI 3 event; however, the potential impacts are far greater. Probabilistic modelling revealed much more widespread tephra fall, with over 770,000 people potentially exposed to 1 kg m^{-2}, and higher tephra loads (>100 kg m^{-2}; ~ >16 cm) closer to the vent (Table 6; Fig. 13c). Tephra falls of up to 100 mm can result in significant impacts such as collapse of power lines and weak structures, damage to non-structural elements on buildings such as guttering and potential collapse of non-engineered and long-span roofs (Table 1; Jenkins et al. 2015). Thicker tephra falls also require more coordinated clean-up response, with remobilisation resulting in repeated clean-up operations (Hayes et al. 2019a).

Many of the rural buildings surrounding Corbetti volcanic system are circular dwellings with grass thatch roofs, or long-span concrete buildings with metal sheet roofs. Field investigations and experimental studies of tephra loading on roofs (i.e., Spence et al. 1996; Blong 2003; Jenkins et al. 2014, 2024b; Hayes et al. 2019b; McSporran 2019) have shown that long-span buildings (characterised by metal sheet roofs resting on purlins, with clear distances of at least 5 m between primary roof supports or trusses; Jenkins et al. 2014) are generally more susceptible to roof collapse than short-span buildings. However, there are several factors that influence this such as condition of the roof material and supports (e.g., Jenkins et al. 2024b), the load distribution across the roof, roof pitch (e.g., Osman et al. 2023), and local building design codes. Tephra fall impact assessment on thatch buildings in the southwest Pacific following the 2017–18 explosive eruption of Manaro Voui volcano on Ambae island, Vanuatu revealed wide variation in damage, from complete collapse under tephra thicknesses of approximately 40 mm, to no damage in areas that experienced 200 mm of tephra deposition (McSporran 2019; Jenkins et al. 2024b). Detailed field investigations found that damage to buildings was influenced by the condition of the buildings (e.g., age of materials and termite damage to structural elements) and rapidly implemented mitigation measures such as addition of roof supports and installation of tarpaulin on thatch roofs which facilitated tephra shedding (McSporran 2019). Similarities can be drawn with buildings around Corbetti, suggesting that in an explosive eruptive event, simple measures such as covering roofs with tarpaulin or other plastic sheeting could help reduce tephra fall impacts. Further work is needed to catalogue building types, construction materials, structural elements, condition of buildings and other factors before any assessment can be made on the vulnerability of buildings surrounding Corbetti volcanic system.

The area surrounding Corbetti is primarily agricultural land with livestock and crop production, including foods for local consumption such as cereals, pulses, tubers, vegetables, and fruits, and market-oriented crop cultivation such as coffee and sugarcane (Morebo et al. 2023). Integration of the Copernicus global land cover data with the probabilistic tephra fall footprints show that just over 2000 km^2 of crop cover lies within 30 km radius of the Corbetti volcanic system, with up to an estimated 135 km^2 of crop cover potentially being impacted by over 100 kg m^{-2} (>16 cm) tephra fall for a VEI 4 explosive event. Recent research has highlighted the lack of data, and hence knowledge of the impacts of tephra fall on agriculture, and the subsequent recovery of vegetation (Biass et al. 2022b). However, observations following eruptions reveal tephra fall can lead to abrasion and shredding of leaves, while thicker tephra falls can lead to smothering and reduced water infiltration resulting in decreased crop production (e.g., Magill et al. 2013; Wilson et al. 2011; Craig et al. 2016). Any explosive event at Corbetti that could produce tephra fall could therefore have significant impacts on agriculture and associated systemic impacts on the economy of the region.

Conclusions

We have probabilistically modelled four explosive event scenarios at the Corbetti volcanic system: VEI 3, 4 and 6 events from the main caldera, and a lower volume off-edifice VEI 2 to 3 event. These represent reasonable likely scenarios based on all the available evidence. We have shown that any explosive event would produce tephra fall that could impact the lives and livelihoods of communities living within and beyond the Corbetti caldera. An explosive event would likely impact geothermal operations within Corbetti caldera and the Hawassa airport, located just 5 km from the Corbetti caldera rim. Agriculture could also be significantly impacted, with, given strong economic dependency on agriculture, potentially significant impacts to the economy. More research is needed to better understand tephra fall impacts on agriculture and related systemic impacts in Ethiopia. The volcanic ash hazard to aviation and from wind remobilisation of ash fall deposits is not accounted for within our modelling. The hazard from airborne ash is likely to affect much larger areas, and hazard from ash remobilisation can continue for months, years or even decades after the event.

These results provide a valuable analysis and visualisation of possible future explosive events, enabling consideration of potential tephra fall impacts, given the current knowledge. These can be used to support decision-making and planning, and to raise awareness of possible impacts from potential future explosive activity in public institutions, regional authorities and local communities. The Ethiopian authors will communicate the results of this study to the Geological Institute of Ethiopia and the Ethiopian Disaster and Risk Management Commission to support their national volcanic hazard and vulnerability assessments. This is particularly important where there are no historical accounts or living memory of eruptive activity.

Supplementary Information

The online version contains supplementary material available at https://doi.org/10.1186/s13617-026-00169-4.

Supplementary material 1

Acknowledgements

We would like to thank the participants of the expert elicitation for giving their time, energy, enthusiasm and knowledge during an intense workshop: Keri McNamara, Ben Clarke and Pablo Tierz. We would also like to thank those who helped us prepare for the elicitation through discussions and meetings but were unable to attend the elicitation: Eliza Calder, David Pyle, Susanna Jenkins and Tamsin Mather. We are grateful to Sebastien Biass for his support with implementing TephraProb and VolcGIS. We are grateful to Jorge Romero and two anonymous reviewers for providing detailed and constructive comments that have greatly improved this manuscript. BGS publishes with permission of the executive director of the British Geological Survey (UKRI).

Author contributions

JC: Data collection, Investigation, Data analysis, Writing – original draft, Writing – review & editing; YB: Investigation, Data analysis, Writing – original draft, Writing – review & editing; SE: Data collection, Investigation, Data analysis, Writing – original draft, Writing – review & editing; KF: Data collection, Writing – review & editing; EL: Conceptualisation, Writing – review & editing; SL: Conceptualisation, Writing – review & editing; AT: Data collection, Writing – review & editing; CVB: Project administration, Conceptualisation, Writing – review & editing; GY: Conceptualisation, Writing – review & editing

Funding

This work was supported by the Natural Environment Research Council (NERC) funded RiftVolc project (NE/L013460/1 and NE/L013932/1), the Global Geological Risk Platform of the British Geological Survey NC-ODA grant NE/R000069/1: Geoscience for Sustainable Futures, BGS International NC programme 'Geoscience to tackle Global Environmental Challenges', NERC reference NE/X006255/1 and the British Geological Survey via NERC national capability.

Data availability

Data are available in the supporting files. For the purpose of open access, the author has applied a Creative Commons Attribution (CC BY) licence to any Author Accepted Manuscript version arising. Maps in Figs. 8–13 were created using ArcGIS® software by Esri. ArcGIS® and ArcMap™ are the intellectual property of Esri and are used herein under license. Copyright © Esri. All rights reserved. For more information about Esri® software, please visit http://www.esri.com.

Declarations

Ethics approval and consent to participate

Not applicable

Consent for publication

All authors confirm that they have read and approved the final version of the manuscript, and consent to its submission for publication in the Journal of Applied Volcanology. Furthermore, the authors affirm that this manuscript has not been previously published, and is not under consideration for publication elsewhere.

Competing interests
The authors declare that they have no competing interests.

Received: 30 July 2025 / Accepted: 26 May 2026
Published online: 02 November 2026

References

Aspinall W (2021) Reminiscences of a Classical Model expert elicitation facilitator. In: Expert judgement in risk and decision analysis. Springer International Publishing, Cham, pp 389–399

Aspinall WP (2006) Structured elicitation of expert judgment for probabilistic hazard and risk assessment in volcanic eruptions. In: Mader HM et al. (eds) Statistics in volcanology. Special publication of IAVCEI. pp 1–31

Aubry TJ, Engwell S, Bonadonna C, Carazzo G, Scollo S, Van Eaton AR, Taylor IA, Jessop D, Eychenne J, Gouhier M, Mastin LG, Wallace KL, Biass S, Bursik M, Grainger RG, Jellinek AM, Schmidt A (2021) The independent volcanic eruption source parameter Archive (IVESPA, version 1.0): a new observational database to support explosive eruptive column model validation and development. J. Volcanol. Geotherm. Res 417:107295. https://doi.org/10.1016/j.jvolgeores.2021.107295

Bedassa G, Ayalew D, Getaneh W, Fontijn K, Emishaw L, Melaku AA, Tadesse AZ, Demissie ZS, Swindle A, Chamberlain KJ (2024) Stratigraphy and eruptive history of Gedemsa caldera volcano, central Main Ethiopian Rift. J. Volcanol. Geotherm. Res 446:107987. https://doi.org/10.1016/j.jvolgeores.2023.107987

Benti NE, Woldegiyorgis TA, Geffe CA, Gurmesa GS, Chaka MD, Mekonnen YS (2023) Overview of geothermal resources utilization in Ethiopia: potentials, opportunities, and challenges. Sci Afr 19:e01562. https://doi.org/10.1016/j.sciaf.2023.e01562

Bernard B, Tadini A, Samaniego P, Bevilacqua A, Vasconez FJ, Aravena A, Vitturi MDM, Hidalgo S (2024) Developing hazard scenarios from monitoring data, historical chronicles, and expert elicitation: a case study of sangay volcano, Ecuador. Bull. Volcanol 86(8):68. https://doi.org/10.1007/s00445-024-01754-4

Biass S, Bonadonna C, Connor L, Connor C (2016) TephraProb: a Matlab package for probabilistic hazard assessments of tephra fallout. J Appl Volcanol 5(1):1–16. https://doi.org/10.1186/s13617-016-0050-5

Biass S, Jenkins SF, Aeberhard WH, Delmelle P, Wilson T (2022a) Insights into the vulnerability of vegetation to tephra falluots from interpretable machine learning and big Earth observation data. Nat Hazards Earth Syst Sci 22(9):2829–2855. https://doi.org/10.5194/nhess-22-2829-2022

Biass S, Williams G, Hayes J, Rui J (2022b) VolcGIS (v1.0), Zenodo [code] https://doi.org/10.5281/zenodo.6416793

Biggs J, Bastow I, Keir D, Lewi E (2011) Pulses of deformation reveal frequently recurring shallow magmatic activity beneath the Main Ethiopian Rift. Geochem Geophys Geosyst 12(9):12. https://doi.org/10.1029/2011GC003662

Blake DM, Deligne NI, Wilson TM, Wilson G (2017) Improving volcanic ash fragility functions through laboratory studies: example of surface transportation networks. J Appl Volcanol 6(1):16. https://doi.org/10.1186/s13617-017-0066-5

Blong R (2003) Building damage in Rabaul. In: Bull Volcanol, vol 65. Papua New Guinea, 1994, pp 43–54. https://doi.org/10.1007/s00445-002-0238-x

Bonadonna C, Connor CB, Houghton BF, Connor L, Byrne M, Laing A, Hincks TK (2005a) Probabilistic modeling of tephra dispersal: hazard assessment of a multiphase rhyolitic eruption at Tarawera, New Zealand. J. Geophys. Res 110(B3):110. https://doi.org/10.1029/2003JB002896

Bonadonna C, Costa A (2013) Modeling of tephra sedimentation from volcanic plumes. Modeling Volcan Processes: Phys Math Volcanism 173–202

Bonadonna C, Costa A, Folch A, Koyaguchi T (2015) Tephra dispersal and sedimentation. In: The encyclopedia of volcanoes. Academic Press, pp 587–597

Bonadonna C, Genco R, Gouhier M, Pistolesi M, Cioni R, Alfano F, Hoskuldsson A, Ripepe M (2011) Tephra sedimentation during the 2010 Eyjafjallajökull eruption (iceland) from deposit, radar, and satellite observations. J. Geophys. Res 116(B12). https://doi.org/10.1029/2011JB008462

Bonadonna C, Phillips JC, Houghton BF (2005b) Modeling tephra sedimentation from a Ruapehu weak plume eruption. J. Geophys. Res 110(B8). https://doi.org/10.1029/2004JB003515

Brown RJ, Hernández W, Escobar D, Gutierrez E, Crummy J, Cole R, Tournigand PY (2022) Reconstruction of the 29th December 2013 eruption of San Miguel volcano, El Salvador, using video, photographs, and pyroclastic deposits. Volcanica 5(2):271–293. https://doi.org/10.30909/vol.05.02.271293

Brown SK, Loughlin SC, Sparks RSJ, Vye-Brown C et al (2015) Global volcanic hazard and risk. In: Loughlin SC et al.eds) Global volcanic hazards a. Cambridge University Press, Cambridge, pp 76–167

Buchhorn M, Smets B, Bertels L, De Roo B, Lesiv M, Tsendbazar NE, Herold M, Fritz S (2020) Copernicus global land service: land cover 100m: collection 3: epoch 2019: globe. Version V3. 0.1. Data Set

Carazzo G, Kaminski E, Tait S (2015) The timing and intensity of column collapse during explosive volcanic eruptions. Earth Planet Sci Lett Feb 411(411):208–217. https://doi.org/10.1016/j.epsl.2014.12.006

Cashman K, Rust A (2016) Introduction: part 2: volcanic ash: generation and spatial variations. In: Volcanic ash: hazard observation. Elsevier Inc, pp 5–22

Clarke B, Calder ES, Dessalegn F, Fontijn K, Cortés JA, Naylor M, Butler I, Hutchison W, Yirgu G (2019) Fluidal pyroclasts reveal the intensity of peralkaline rhyolite pumice cone eruptions. Nat Commun 10(1):1–10. https://doi.org/10.1038/s41467-019-09947-8

Clarke B, Tierz P, Calder E, Yirgu G (2020) Probabilistic volcanic hazard assessment for pyroclastic density currents from pumice cone eruptions at Aluto volcano, Ethiopia. Front Earth Sci 8. https://doi.org/10.3389/feart.2020.00348

Colby DJ (2023) Eruptive history and magmatic evolution of Corbetti Caldera in the main Ethiopian rift (Doctoral dissertation, University of Oxford

Colby DJ, Pyle DM, Fontijn K, Mather TA, Melaku AA, Mengesha MA, Yirgu G (2022) Stratigraphy and eruptive history of Corbetti Caldera in the Main Ethiopian Rift. J. Volcanol. Geotherm. Res 428:107580. https://doi.org/10.1016/j.jvolgeores.2022.107580

Cole PD, Queiroz G, Wallenstein N, Gaspar JL, Duncan AM, Guest JE (1995) An historic subplinian/phreatomagmatic eruption: the 1630 AD eruption of Furnas volcano, sa˜ o Miguel, Azores. J. Volcanol. Geotherm. Res 69(1–2):117–135. https://doi.org/10.1016/0377-0273(95)00033-X

Connor CB, Hill BE, Winfrey B, Franklin NM, Femina PCL (2001) Estimation of volcanic hazards from tephra fallout. Nat Hazards Rev 2(1):33–42. https://doi.org/10.1061/(ASCE)1527-6988(2001)2:1(33)

Connor LJ, Connor CB (2006) Inversion is the key to dispersion: understanding eruption dynamics by inverting tephra fallout

Constantinescu R, White JT, Connor CB, Hopulele-Gligor A, Charbonnier S, Thouret JC, Lindsay JM, Bertin D (2022) Uncertainty quantification of eruption source parameters estimated from tephra fall deposits. Geophys Res Lett 49(6):e2021GL097425. https://doi.org/10.1029/2021GL097425

Craig H, Wilson T, Stewart C, Villarosa G, Outes V, Cronin S, Jenkins S (2016) Agricultural impact assessment and management after three widespread tephra falls in Patagonia, south America. Nat Hazards. 2016 Jun; 82(2):1167–1229. https://doi.org/10.1007/s11069-016-2240-1

Crummy JM, Marchant B, Loughlin SC, Engwell S, Tierz P, Cuba DM, Vye-Brown C (2018) Elicitation of potential future explosive silicic eruption scenarios at Corbetti and Aluto volcanoes, Ethiopia. Br Geological Survey Open File Report OR/18/061. 66pp

Dambly ML, Samrock F, Grayver A, Eysteinsson H, Saar MO (2024) Geophysical imaging of the active magmatic intrusion and geothermal reservoir formation beneath the Corbetti prospect, Main Ethiopian Rift. Geophys J Int 236(3):1764–1781. https://doi.org/10.1093/gji/ggad493

Dee DP, Uppala S, Simmons AJ, Berrisford P, Poli P, Kobayashi S, Andrae U, Balmaseda MA, Balsamo G, Bauer DP, Bechtold P, Beljaars ACM, van de Berg L, Bidlot J, Bormann N, Delsol C, Dragani R, Fuentes M, Geer AJ, Haimberger L, Healy SB, Hersbach H, Hólm EV, Isaksen L, Kållberg P, Köhler M, Matricardi M, McNally AP, Monge-Sanz BM, Morcrette J-J, Park B-K, Peubey C, de Rosnay P, Tavolato C, Thépaut J-N, Vitart F (2011) The ERA-Interim reanalysis: configuration and performance of the data assimilation system. Quart J R Meteoro Soc 137(656):553–597. https://doi.org/10.1002/qj.828

Di Paola GM (1971) Geology of the Corbetti caldera area (Main Ethiopian Rift valley). Bull. Volcanol 35(2):497–506. https://doi.org/10.1007/BF02596970

Ethiopian Public Health Institute (2021) Ethiopia Mini demographic and health Survey, 2019: final Report. Technical report, EPHI and ICF, Rockville, Maryland, USA. ISBN: 2511127547

Ethiopian Statistical Service (2023) Population size by sex, area and density by region, zone and Wereda: July 2023. Available at http://www.statsethiopia.gov.et/population-projection/. Accessed 16 July 2025

Fernandez-Turiel JL, Saavedra J, Perez-Torrado FJ, Rodriguez-Gonzalez A, Carracedo JC, Lobo A, Rejas M, Gallardo JF, Osterrieth M, Carrizo J, Esteban G (2015) April. The ash deposits of the 4200 BP Cerro Blanco eruption: the largest Holocene eruption of the central Andes. In EGU General Assembly Conference Abstracts, pp 3392

Fontijn K, Ernst GGJ, Bonadonna C, Elburg MA, Mbede E, Jacobs P (2011) The~ 4-ka Rungwe pumice (south-western Tanzania): a wind-still Plinian eruption. Bull. Volcanol 73(9):1353–1368. https://doi.org/10.1007/s00445-011-0486-8

Fontijn K, McNamara K, Tadesse AZ, Pyle DM, Dessalegn F, Hutchison W, Mather TA, Yirgu G (2018) Contrasting styles of post-caldera volcanism along the Main Ethiopian Rift: implications for contemporary volcanic hazards. J. Volcanol. Geotherm. Res 356:90–113. https://doi.org/10.1016/j.jvolgeores.2018.02.001

Global Volcanism Program (2024) [Database] volcanoes of the world (v. 5.2.4; 21 Oct2024). Distrib Smithson Institution, compiled by Venzke, E. https://doi.org/10.5479/si.GVP.VOTW5-2024.5.2

Gudmundsdóttir ER, Larsen G, Björck S, Ingólfsson Ó, Striberger J (2016) A new high-resolution Holocene tephra stratigraphy in eastern Iceland: improving the Icelandic and north Atlantic tephrochronology. Quaternary Sci Rev 150:234–249. https://doi.org/10.1016/j.quascirev.2016.08.011

Hasenaka T, Wibowo HE, Kurniawan IA, Connor C, Connor L, Kiyosugi K, Bonadonna C (2011) Tephra fallout model and grain size distribution of shinmoe-dake tephra, 2011 eruption of Kirishima volcano. In Japan Geoscience Union Meeting, pp 22–27

Hayes JL, Biass S, Jenkins SF, Meredith ES, Williams GT (2022) Integrating criticality concepts into road network disruption assessments for volcanic eruptions. J Appl Volcanol 11(1):8. https://doi.org/10.1186/s13617-022-00118-x

Hayes JL, Calderón R, Deligne NI, Jenkins SF, Leonard GS, McSporran AM, Williams GT, Wilson TM (2019a) Timber-framed building damage from tephra fall and lahar: 2015 Calbuco eruption, Chile. J. Volcanol. Geotherm. Res 374:142–159. https://doi.org/10.1016/j.jvolgeores.2019.02.017

Hayes JL, Wilson TM, Stewart C, Villarosa G, Salgado P, Beigt D, Outes V, Deligne NI, Leonard GS (2019b) Tephra clean-up after the 2015 eruption of Calbuco volcano, Chile: a quantitative geospatial assessment in four communities. J Appl Volcanol 8(1):1–23. https://doi.org/10.1186/s13617-019-0087-3

Hilemichaeil S, Haile T, Yirgu G (2024) Integrated geophysical methods to constrain subsurface structures of tulu Moye-Bora-berecha axial volcanic complex, main Ethiopia rift: implications for geothermal resources. Heliyon 10(7):e28499. https://doi.org/10.1016/j.heliyon.2024.e28499

Horwell CJ, Baxter PJ (2006) The respiratory health hazards of volcanic ash: a review for volcanic risk mitigation. Bull. Volcanol 69(1):1–24. https://doi.org/10.1007/s00445-006-0052-y

Hutchison W, Biggs J, Mather TA, Pyle DM, Lewi E, Yirgu G, Caliro S, Chiodini G, Clor LE, Fischer TP (2016a) Causes of unrest at silicic calderas in the east African Rift: new constraints from InSAR and soil-gas chemistry at Aluto volcano, Ethiopia. Geochem Geophys Geosyst 17(8):3008–3030. https://doi.org/10.1002/2016GC006395

Hutchison W, Pyle DM, Mather TA, Yirgu G, Biggs J, Cohen BE, Barfod DN, Lewi E (2016b) The eruptive history and magmatic evolution of Aluto volcano: new insights into silicic peralkaline volcanism in the Ethiopian rift. J. Volcanol. Geotherm. Res 328:9–33. https://doi.org/10.1016/j.jvolgeores.2016.09.010

InfraCo Africa (2023) Geothermal Corbetti project.https://infracoafrica.com/project/corbetti/. 28th April 2023

Jenkins SF, Biass S, Williams GT, Hayes JL, Tennant E, Yang Q, Burgos V, Meredith ES, Lerner GA, Syarifuddin M, Verolino A (2022) Evaluating and ranking Southeast Asia's exposure to explosive volcanic hazards. Nat Hazards Earth Syst Sci 22(4):1233–1265. https://doi.org/10.5194/nhess-22-1233-2022

Jenkins SF, Magill CR, McAneney KJ (2007) Multi-stage volcanic events: a statistical investigation. J. Volcanol. Geotherm. Res 161(4):275–288. https://doi.org/10.1016/j.jvolgeores.2006.12.005

Jenkins SF, McSporran A, Wilson TM, Stewart C, Leonard G, Cevuard S, Garaebiti E (2024a) Tephra fall impacts to buildings: the 2017–2018 Manaro Voui eruption, Vanuatu. Front Earth Sci 12:1392098. https://doi.org/10.3389/feart.2024.1392098

Jenkins SF, Mee K, Engwell S, Loughlin S, Faria B, Yirgu G, Bekele Y, Lewi E, Vye-Brown C, Fraser S, Day S, Lark RM, Huyck C, Crummy J (2024b) Assessing volcanic hazard and exposure in data poor environments for International stakeholders: case study for Ethiopia, Kenya, and Cabo Verde. Kenya Cabo Verde

Jenkins SF, Spence RJ, Fonseca JF, Solidum RU, Wilson TM (2014 Apr) Volcanic risk assessment: quantifying physical vulnerability in the built environment. J. Volcanol. Geotherm. Res 276(276):105–120. https://doi.org/10.1016/j.jvolgeores.2014.03.002

Jenkins SF, Wilson TM, Magill C, Miller V, Stewart C, Blong R, Marzocchi W, Boulton M, Bonadonna C, Costa A (2015) Volcanic ash fall hazard and risk. In: Loughlin SC, Sparks S, Brown SK, Jenkins SF, Vye-Brown C (eds) Global volcanic hazards. Cambridge University Press, and Risk, pp 173–222

Jude-Eton TC, Thordarson T, Gudmundsson MT, Oddsson B (2012) Dynamics, stratigraphy and proximal dispersal of supraglacial tephra during the ice-confined 2004 eruption at Grímsvötn volcano, Iceland. Bull. Volcanol 74(5):1057–1082. https://doi.org/10.1007/s00445-012-0583-3

Lewi E, Biggs J, Ayele A, Wright T, Pagli C, Keir D, Ali Y, Assefa G, Wang H, La Rosa A, Way L, Mengistu F, Loughlin S, Grandin R, Temtime T, Birhanu Y, Freymueller J, Zheng W (2025) Scientific response to the 2024–2025 dyke intrusions in the Fentale-Dofen region, Ethiopia: geophysical monitoring, surface manifestations, and hazard mapping. Bull. Volcanol 87(8):64. https://doi.org/10.1007/s00445-025-01852-x

Limberger F, Alemayehu S, Rümpker G, Ayele A (2026) Seismic signature of the 23 November 2025 Hayli Gubbi eruption sequence in Afar, Ethiopia. Authorea Pre-Print. January 12, 2026

Magill C, Wilson T, Okada T (2013) Observations of tephra fall impacts from the 2011 shinmoedake eruption, Japan. Earth Planet Sp 65(6):677–698. https://doi.org/10.5047/eps.2013.05.010

Martin-Jones CM, Lane CS, Pearce NJG, Smith VC, Lamb HF, Schaebitz F, Viehberg F, Brown MC, Frank U, Asrat A (2017) Recurrent explosive eruptions from a high-risk Main Ethiopian Rift volcano throughout the Holocene. Geology 45(12):1127–1130. https://doi.org/10.1130/G39594.1

McNamara K, Cashman KV, Rust AC, Fontijn K, Chalié F, Tomlinson EL, Yirgu G (2018) Using lake sediment cores to improve records of volcanism at Aluto volcano in the Main Ethiopian Rift. Geochem Geophys Geosyst 19(9):3164–3188. https://doi.org/10.1029/2018GC007686

McSporran AM (2019) Impacts of tephra fall on buildings from the 2017–2018 eruption of Manaro Voui volcano. Ambae Island, Vanuatu

Michaud-Dubuy A, Komorowski JC, Carazzo G (2025) Tephra fallout and dispersal modeling of phreatic eruptions: implications for volcanic hazard assessment in Martinique and Guadeloupe (lesser antilles). Bull. Volcanol 87(2):11. https://doi.org/10.1007/s00445-025-01795-3

Morebo MT, Maja MM, Lakew AA (2023) Impact of climate variability on maize (zea mays L.) yield and Farmers' adaptation strategies in Hawassa Zuria District, Sidama region, Ethiopia. AJEP 12(5):121–137. https://doi.org/10.11648/j.ajep.20231205.11

NASA/METI/AIST/Japan Spacesystems and U.S./Japan ASTER Science Team (2009) ASTER Global digital elevation model. NASA Land Processes Distributed Active Archive Center. https://doi.org/10.5067/ASTER/ASTGTM.002 Date Accessed:06/10/2018

Nelder JA, Mead R (1965) A simplex method for function minimization. Comput J 7(4):308–313. https://doi.org/10.1093/comjnl/7.4.308

NOAA (2015) NCEP-NOAA reanalysis 2 wind data. In NOAA/ESRL/PSD, Ed. http://www.esrl.noaa.gov/psd/data/gridded/data.ncep.reanalysis2.html

O'Hagan A (2019) Expert knowledge elicitation: subjective but scientific. Am J Intellect Dev Disabil Statistician 73(sup1):69–81. https://doi.org/10.1080/00031305.2018.1518265

Oakley JE, O'Hagan A (2010) SHELF: the Sheffield elicitation framework (version 2.0). School of Mathematics and Statistics, University of Sheffield, Sheffield, UK, p 560

Osman S, Thomas M, Crummy J, Sharp A, Carver S (2023) Laboratory tests to understand tephra sliding behaviour on roofs. J Appl Volcanol 12(1):11. https://doi.org/10.1186/s13617-023-00137-2

Pyle DM (1989) The thickness, volume and grainsize of tephra fall deposits. Bull. Volcanol 51(1):1–15. https://doi.org/10.1007/BF01086757

Rapprich V, Žáček V, Verner K, Erban V, Goslar T, Bekele Y, Legesa F, Hroch T, Hejtmánková P (2016) Wendo Koshe Pumice: the latest Holocene silicic explosive eruption product of the Corbetti volcanic system (southern Ethiopia). J. Volcanol. Geotherm. Res 310:159–171. https://doi.org/10.1016/j.jvolgeores.2015.12.008

Romero JE, Morgavi D, Arzilli F, Daga R, Caselli A, Reckziegel F, Viramonte J, Díaz-Alvarado, Polacci M, Burton M, Perugini D, Díaz-Alvarado J (2016) Eruption dynamics of the 22–23 April 2015 Calbuco volcano (southern Chile): analyses of tephra fall deposits. J. Volcanol. Geotherm. Res 317:15–29. https://doi.org/10.1016/j.jvolgeores.2016.02.027

Rose A, McKee J, Sims K, Bright E, Reith A, Urban M (2020) LandScan Global 2019. Oak Ridge National Laboratory. https://doi.org/10.48690/1524214 [Data set

Scollo S, Bonadonna C, Garcia A, Mereu L, Prestifilippo M, Romeo F, Sandri L, Stocchi M (2025) New developments in the estimation of tephra fallout hazard at Mt. Etna, in Italy, during the PANACEA project. Ann Geophysics 68(1):1–17. https://doi.org/10.4401/ag-9174

Scollo S, Tarantola S, Bonadonna C, Coltelli M, Saltelli A (2008) Sensitivity analysis and uncertainty estimation for tephra dispersal models. J. Geophys. Res 113(B6). https://doi.org/10.1029/2006JB004864

Siegburg M, Gernon TM, Bull JM, Keir D, Barfod DN, Taylor RN, Abebe B, Ayele A (2018) Geological evolution of the boset-bericha volcanic complex, Main Ethiopian Rift: 40 Ar/39 Ar evidence for episodic pleistocene to Holocene volcanism. J. Volcanol. Geotherm. Res 351:115–133. https://doi.org/10.1016/j.jvolgeores.2017.12.014

Spence RJS, Pomonis A, Baxter PJ, Coburn AW, White M, Dayrit M (1996) Building damage caused by the Mt. Pinatubo eruption of June 14-15, 1991. In: Newhall CG, Punongbayan R (eds) Fire and mud: eruptions and lahars of mount Pinatubo. University of Washington Press, Philippines

Stevenson JA, Loughlin S, Rae C, Thordarson T, Milodowski AE, Gilbert JS, Harangi S, Lukács R, Højgaard B, Árting U, Pyne-O'Donnell S, MacLeod A, Whitney B, Cassidy M (2012) Distal deposition of tephra from the Eyjafjallajökull 2010 summit eruption. J. Geophys. Res 117(B9). https://doi.org/10.1029/2011JB008904

Styron R, Pagani M (2020) The GEM global active faults database. Earthquake Spectra 36(1S):160–180. https://doi.org/10.1177/8755293020944182

Suzuki T (1983) A theoretical model for dispersion of tephra. In: Shimozuru D, Yokoyama I (eds) Arc volcanism: physics and tectonics. Terra Scientific Publishing, Tokyo, pp 95–116

Tadesse AZ, Bedassa G, Kervyn M, Muluneh AA, Gudbrandsson S, Yirgu G, Ayalew D, Fontijn K (2023a) Structural controls on magma pathways in Bora-Baricha-Tullu Moye (BBTM) volcanic system, Main Ethiopian Rift. Main Ethiopian Rift Volcanica 6(2):367–390. https://doi.org/10.30909/vol.06.02.367390

Tadesse AZ, Fontijn K, Caricchi L, Begue F, Gudbrandsson S, Smith VC, Gopon P, Debaille V, Laha P, Terryn H, Yirgu G, Ayalew D (2023b) Pre-eruptive storage conditions and magmatic evolution of the Bora-Baricha-Tullu Moye volcanic system, Main Ethiopian Rift. Lithos 442-443:107088. https://doi.org/10.1016/j.lithos.2023.107088

Tadesse AZ, Fontijn K, Melaku AA, Gebru EF, Smith VC, Tomlinson E, Barfod D, Gopon P, Bégué F, Caricchi L, Laha P, Terryn H, Gudbrandsson S, Yirgu G, Ayalew D (2022) Eruption frequency and magnitude in a geothermally active continental rift: the Bora-Baricha-Tullu Moye volcanic complex, Main Ethiopian Rift. J. Volcanol. Geotherm. Res 423:107471. https://doi.org/10.1016/j.jvolgeores.2022.107471

Tierz P, Clarke B, Calder ES, Dessalegn F, Lewi E, Yirgu G, Fontijn K, Crummy JM, Bekele Y, Loughlin SC (2020) Event trees and epistemic uncertainty in long-term volcanic hazard assessment of rift volcanoes: the example of Aluto (central Ethiopia). Geochem Geophys Geosyst 21(10):e2020GC009219. https://doi.org/10.1029/2020GC009219

Tierz P, Loughlin SC, Calder ES (2019) VOLCANS: an objective, structured and reproducible method for identifying sets of analogue volcanoes. Bull. Volcanol 81(12):76. https://doi.org/10.1007/s00445-019-1336-3

Vye-Brown C, Brown RJ, Crummy JM, Engwell S, Loughlin SC (2019) Volcanic history and future hazards affecting ascension Island. Br Geological Survey Open File Report OR/19/026

Vye-Brown C, Sparks R, Lewi E, Mewa G, Asrat A, Loughlin S, Mee K, Wright T (2016) Ethiopian volcanic hazards: a changing research landscape: geological Society, vol 420. Special Publications, London, pp 355–365

Watts EJ, Gernon TM, Taylor RN, Keir D, Siegburg M, Jarman J, Pagli C, Gioncada A (2020) Evolution of the alu-dalafilla and borale volcanoes, Afar, Ethiopia. J. Volcanol. Geotherm. Res 408:107094. https://doi.org/10.1016/j.jvolgeores.2020.107094

Way L, Biggs J, Zheng W, Lazecky M, Dualeh EW, Wright T, Grandin R, Hauck A, Loughlin S, Crummy J, Lewi E (2025) Real-time satellite monitoring of the 2024–2025 dyke intrusion sequence at Fentale-Dofen volcanoes, Ethiopia. Bull. Volcanol 87(11):100. https://doi.org/10.1007/s00445-025-01884-3

Williams CJ, Wilson KJ, Wilson N (2021) A comparison of prior elicitation aggregation using the classical method and SHELF. J R Stat Soc Ser A: Stat Soc 184(3):920–940. https://doi.org/10.1111/rssa.12691

Wilson T, Cole J, Cronin S, Stewart C, Johnston D (2011) Impacts on agriculture following the 1991 eruption of Vulcan Hudson, Patagonia: lessons for recovery. Nat Hazards 57(2):185–212. https://doi.org/10.1007/s11069-010-9604-8

Wuletawu H, Alemu A, Nigussie W, Mickus K, Keir D, Wendwesen S, Wassihun S (2024) The subsurface anatomy of a mid-upper crustal magmatic intrusion zone beneath the Boku volcanic complex, Main Ethiopian Rift inferred from gravity data. J. Volcanol. Geotherm. Res 452:108133. https://doi.org/10.1016/j.jvolgeores.2024.108133

Yang Q, Pitman EB, Bursik M, Jenkins SF (2021) Tephra deposit inversion by coupling Tephra2 with the Metropolis-Hastings algorithm: algorithm introduction and demonstration with synthetic datasets. J Appl Volcanol 10(1):1. https://doi.org/10.1186/s13617-020-00101-4

Yirgu G, Ferguson DJ, Barnie TD, Oppenheimer C (2014) Recent volcanic eruptions in the Afar rift, northeastern Africa, and implications for volcanic risk management in the region. Extreme natural hazards, disaster risks and societal implications. Cambridge University Press, Cambridge, pp 200–213

Publisher's Note

Springer Nature remains neutral with regard to jurisdictional claims in published maps and institutional affiliations.